Gadoxetic Acid-enhanced Liver MRI: Everything You Need to Know

Gadoxetic Acid-enhanced Liver MRI: Everything You Need to Know

Shintaro Ichikawa*, MD, PhD, Satoshi Goshima, MD, PhD

Department of Radiology, Hamamatsu University School of Medicine

*Corresponding author: Shintaro Ichikawa

Department of Radiology, Hamamatsu University School of Medicine

1-20-1 Handayama, Higashi-ku, Hamamatsu, Shizuoka 431-3192, Japan

Phone +81-53-435-2242, Fax +81-53-435-2241

Email: shintaro@hama-med.ac.jp

Running title: Gadoxetic Acid-enhanced Liver MRI

Keywords: magnetic resonance imaging, gadoxetic acid, liver, hepatocellular carcinoma, hepatobiliary phase

Conflicts of Interest and Source of Funding:

The authors declare that they have no conflicts of interest.

Gadoxetic Acid-enhanced Liver MRI: Everything You Need to Know

Abstract

Since its introduction in the worldwide medical market, gadoxetic acid has attracted considerable interest. The year 2023 marks the 15th anniversary of the introduction of gadoxetic acid in Japan. Gadoxetic acid-enhanced magnetic resonance imaging (GA-MRI) is the predominantly performed contrast MRI examination for the liver. Its most essential characteristic, namely the hepatobiliary phase, revolutionized the clinical management of liver disease. GA-MRI is currently the most efficient method for focal liver lesion detection and analysis. Meta-analyses demonstrated its excellent effectiveness for the diagnosis of hepatocellular carcinoma and liver metastases. Owing to the extensive usage of gadoxetic acid, a hepatobiliary phase hypointense nodule without arterial phase hyperenhancement is well documented. The existence of such nodules may be a sign of hypervascular hepatocellular carcinoma in nodules and other areas in the liver. Apart from its role in tumor identification and characterization, GA-MRI can help assess response to therapy and liver fibrosis. Therefore, it is proposed to use gadoxetic acid as the first option for MRI of the liver in the majority of patients. The efficacy of gadoxetic acid surpasses its disadvantages, rendering this contrast agent the preferred choice for routine MRI of the liver. The clinical use of GA-MRI is discussed in this review article.

Key words: magnetic resonance imaging, gadoxetic acid, liver, hepatocellular carcinoma, hepatobiliary phase

Introduction

Chronic liver disease (CLD) ranks among the 10 major causes of mortality globally, accounting for nearly 2 million deaths each year; in addition, the incidence rate of CLD is increasing.[1] Hepatitis B and C viruses are commonly responsible for the development of CLD; other causes of CLD include nonalcoholic fatty liver disease and nonalcoholic steatohepatitis. Cirrhosis is strongly associated with hepatocellular carcinoma (HCC), regardless of the disease origin.[2] Although efficacious drug therapy for viral hepatitis (particularly hepatitis C) has been developed, HCC continues to pose a major clinical challenge owing to the increasing incidence of nonalcoholic fatty liver disease and nonalcoholic steatohepatitis. Furthermore, the expanded life expectancy and medical advancements have rendered long-term survival feasible for patients with cancer, thereby increasing the incidence of metastatic liver cancer.

Magnetic resonance imaging (MRI) is widely used for the detection of liver disorders. Over the years, this method has been substantially improved. Compared with computed tomography (CT), MRI provides a greater number of benefits for the diagnosis of liver disease, including superior contrast resolution, no exposure to radiation, and two distinct contrast agents (extracellular and hepatocyte-specific). Additionally, MRI yields morphological and quantitative data. Gadoxetic acid (GA) is a hepatocyte-specific contrast agent; Sweden was the first country to approve its use in 2004, followed by Japan in 2007 and the United States of America in 2008. Thus, GA-enhanced MRI (GA-MRI) has been used for 15 and 20 years in Japan and worldwide, respectively. Due to its excellent effectiveness in lesion detection and analysis, GA is primarily used in Japan for MRI of the liver.[3,4] GA-MRI offers higher diagnostic accuracy versus contrast-enhanced CT (CE-CT). Despite its drawbacks, GA is currently the preferred contrast agent for routine MRI of the liver. To ensure appropriate diagnosis and management of focal liver disorders, it is essential to comprehend the features of the contrast medium. The features of this contrast agent, imaging methods, diagnostic value, and applications are discussed in thie review article.

Imaging Techniques of GA-MRI

Dynamic MRI

Following intravenous administration, GA acts as an extracellular contrast agent in the arterial phase (AP) and portal venous phase (PVP). Subsequently, GA is uptaken by hepatocytes. Therefore, hepatobiliary phase (HBP) images are captured 15–20 min after the administration, which is the most important feature of GA-MRI. Typically, GA-MRI is acquired through a fat-suppressed three-dimensional gradient echo sequence. This approach is linked to excellent spatial resolution and signal-to-noise ratio. Dynamic MRI images are captured prior to (pre-contrast), and 20–30 s (AP), 1–2 min (PVP), 2–5 min (transitional phase, TP), and 15–20 min (HBP) following the administration of GA. The administration of GA is performed intravenously as a bolus (rate: 1 mL/s) through an intravenous cubital line. Saline (20 mL) is used to flush the line using a power injector. AP images are captured with a fluoroscopic triggering technique. The definitions of all phases, as they appear in the Liver Imaging Reporting and Data System version 2018 (LI-RADS v2018) are provided below.[5]

- AP (late AP): Post-contrast injection period: i) hepatic artery and branch full enhancement; and ii) no hepatic vein enhancement by antegrade flow (Figure 1).
- PVP: Post-contrast injection period: i) portal vein full enhancement; ii) hepatic vein enhancement by antegrade flow; and iii) liver parenchyma full enhancement.
- TP: Post-contrast injection phase between the PVP and HBP: i) similar signal intensity for liver vessels and hepatic parenchyma; and ii) substantial contributions of the agent (intracellular and extracellular amounts) to parenchyma enhancement.
- HBP: Post-contrast injection phase with the following features: i) hyperintense liver parenchyma compared with hepatic blood vessels; and ii) contrast agent excretion into the biliary system.

AP images are important for focal liver lesion detection. Differential diagnosis depends on the nature of the lesion (i.e., hypervascular, hypovascular, or without contrast effect). PVP images are necessary for assessing portal blood flow in focal liver lesions, because the portal blood flow in HCC varies with the stage of carcinogenesis. TP is the phase following PVP. The term “equilibrium phase”, which is used in dynamic study with extracellular gadolinium-based contrast agents (GBCAs), is inappropriate for GA-MRI. This is because the amount of GA in GA-MRI is constantly greater in the liver parenchyma versus the vasculature (i.e., it is never at equilibrium). The uptake of GA by focal

liver lesions is an important parameter in the HBP. This is because it can help detect functioning hepatocytes in the lesion.

Additional imaging modalities

To improve the diagnostic accuracy, apart from dynamic imaging, it is essential to obtain T1-weighted in- and opposed-phase images, T2-weighted images (T2WI), and diffusion-weighted images (DWI). The amount of fat in focal liver lesions, e.g., angiomyolipoma, hepatocellular adenoma (HCA), and HCC, is evaluable by comparing the signal reduction on opposed- and in-phase images. In addition to conventional fat-suppressed T2WI, a heavily T2WI at echo time >150 ms can help differentiate cysts and hemangiomas with long T2 values from malignant tumors (Figure 2).[6] DWI is a useful sequence for identifying focal liver lesions (b-value = 800 or 1,000 s/mm^2 is recommended). Before dynamic study, T1-weighted in- and opposed-phase images and pre-contrast fat-suppressed T1-weighted images (T1WI) are acquired. It is possible to reduce the examination time for GA-MRI by acquiring T2WI and DWI between the dynamic study and HBP.[7]

Clinical Significance for Focal Liver Lesions

Diagnosis of hypervascular HCC

The arterial phase hyperenhancement (APHE) and subsequent washout are characteristics of hypervascular HCC. Enhancing capsules can be detected in the PVP and TP. Typical cases show moderate hyperintensity on T2WI and restricted diffusion. T1-weighted in- and opposed-phase images may reveal intratumoral fat (Figure 3). Owing to the high organic anion transporting polypeptide 1B3 (OATP1B3) expression, ~10% of HCCs exhibit hyperintensity (Figure 4), whereas the majority of HCCs exhibit hypointensity in the HBP. OATP1B3 is the primary uptake transporter of GA in HCC.[8] Meta-analyses demonstrated that the pooled sensitivity and specificity for HCC diagnosis through GA-MRI were 0.85–0.92 and 0.89–0.96,[9–17] respectively. In other research studies, GA-MRI exhibited excellent ability for HCC (<2 cm) diagnosis, with sensitivities ranging from 0.79 to 0.94.[9–11] Particularly for small HCCs, GA-MRI offers greater diagnostic accuracy versus CE-CT (Figure 5). In addition, the SORAMIC study revealed that GA-MRI accurately detects multiple HCCs (>4 lesions)

compared with CE-CT, thereby facilitating the selection of treatment strategies.[18]

GA-MRI is also beneficial for assessing microvascular invasion (MVI), which indicates disease aggressiveness and poor survival in HCC. MVI refers to tumor cell invasion in the vascular endothelium, that is exclusively visible through microscopy. GA-MRI may be applicable, as it displays peritumoral arterial enhancement, non-smooth tumor margin, and peritumoral hypointensity on the HBP as indicators of MVI (Figure 6). According to a meta-analysis, the pooled sensitivity and specificity of peritumoral arterial enhancement were 0.50 and 0.80, respectively, while these values for peritumoral hypointensity during the HBP were 0.55 and 0.87, respectively.[19] Thus, GA-MRI exhibits poor sensitivity, but good specificity for the identification of MVI.

The guidelines established by the Japan Society of Hepatology (JSH) advocate liver resection or locoregional treatment based on the early identification of HCC;[20] hence, sensitivity has been traditionally crucial in Japan. However, liver transplantation is commonly performed in the United States of America and Europe; therefore, specificity is also essential. The criteria for HCC diagnosis are consistent with this notion. HBP hypointensity is equated to washout in the JSH guideline;[20] nevertheless, the LI-RADS v2018 specifies that the evaluation of the washout should only be performed during the PVP.[20] In Japanese individuals at high risk of HCC development, Nishie et al. observed that GA-MRI was more cost-effective versus GBCA-enhanced MRI or CE-CT.[21] Widespread utilization of GA-MRI might lower HCC-related health care expenses, particularly treatment costs.

HBP hypointense nodule without APHE

Nodules appearing hypovascular in the AP and hypointense in the HBP are frequently observed in patients with CLD. Recently, the term “HBP hypointense nodule without APHE” has been used to describe such nodules.[22] They are categorized as borderline nodules, with dysplastic nodules and early HCCs serving as indicators of hypervascular HCC in patients with CLD (Figure 7). A meta-analysis revealed hypervascularization in 28.2% of these nodules.[23] A baseline tumor size >9–10 mm, restricted diffusion, T2 hyperintensity, and previous HCC history were identified as risk factors for hypervascularization.[23,24] Surprisingly, in a South Korean multicenter study, 44.0% of HBP

hypointense nodules without APHE were pathologically identified as advanced HCC; other types included early HCC, high- or low-grade dysplastic nodules, and regenerative nodules.[25]

On pretreatment MRI, HBP hypointense nodules without APHE are also an important risk factor for HCC recurrence following curative therapy. HBP hypointense nodules without APHE are indicative of disease recurrence following HCC surgery.[26,27] According to a meta-analysis, patients with these nodules had an overall pooled hazard ratio of 2.44 for the recurrence of intrahepatic distant disease after hepatectomy or ablation.[28] Apart from a simple precursor of hypervascular HCC, these nodules can serve as a biomarker of hepatocarcinogenesis in the whole liver (Figure 8).[29–31]

Diagnosis of liver metastases

Prior to initiating therapy for colorectal adenocarcinoma, it is vital to precisely determine liver metastases. This is because surgery is recommended when liver metastases are completely resectable. GA-MRI exhibits higher effectiveness versus CE-CT in the detection of colorectal liver metastases (Figure 9).[32] In a study, the combination of GA-MRI with CE-CT changed the intended surgical strategy in 33% of cases.[33] Combined DWI and HBP examinations offer the best sensitivity for detecting liver metastases, especially those of small size. Data from a meta-analysis revealed that the sensitivity of DWI, HBP, and their combination was 0.87, 0.91, and 0.96 (all lesions) and 0.69, 0.83, and 0.91 (metastases <1 cm), respectively.[34] In the VALUE trial, GA-MRI was recommended as the initial imaging method for evaluating hepatic resectability in patients with colorectal liver metastases.[35,36] In terms of diagnostic ability, GA-MRI was better versus CE-CT and extracellular GBCA-enhanced MRI, with higher diagnostic confidence.[35] A change in surgical plan during surgery was less frequently recorded in the GA-MRI group (28%) versus the extracellular GBCA-enhanced MRI (32%) and CE-CT (47%) groups.[35] In terms of eligibility for potentially curative surgery, more patients were eligible in the GA-MRI group (39.3%) versus the extracellular GBCA-enhanced MRI (31.0%) and CE-CT (26.7%) groups. Moreover, GA-MRI was associated with reduced requirement for additional imaging and similar cost for diagnostic examinations versus other methods.[36]

Furthermore, GA-MRI is able to identify liver metastases of pancreatic ductal adenocarcinoma (PDAC). Surgical resection of PDAC is contraindicated following the detection of liver metastases

through imaging. GA-MRI is equivalent to CE-CT in depicting PDAC and exhibits higher sensitivity for detecting liver metastases, especially those of small size. On CE-CT or MRI, consistent with colorectal liver metastases, PDAC metastatic tumors often demonstrate early rim enhancement and delayed inner area enhancement. Occasionally, we encounter instances of misdiagnosis of liver metastases as microabscesses or pseudolesions due to their initial appearance as arterioportal shunts. HBP images demonstrate low signal intensity for this type of metastasis (Figure 10).[37]

Most liver metastases are hypovascular because colorectal and pancreas are common primary sites. However, hypervascular cancers (e.g., neuroendocrine neoplasm, renal cell carcinoma, melanoma, gastrointestinal stromal tumors) may induce hypervascular liver metastases (Figure 11). HCC and hypervascular liver metastases have distinct risk factors. Nevertheless, distinguishing HCC from hypervascular liver metastases through imaging may be difficult when the latter show non-rim APHE. GA-MRI can assist in differentiating these two types of lesions; in particular, non-peripheral washout and the mosaic architecture can be reliably used to distinguish HCC from hypervascular liver metastases through imaging.[38]

Distinguishing between HCA and focal nodular hyperplasia (FNH)

HCA and FNH are often contrasted because of their similarities, such as a predilection for young women without CLD, association with oral contraceptives, and hypervascularity. The two most useful imaging findings for differentiating FNH from HCA are discussed below.

- Central scar

  The central scar in FNH is composed of blood vessels and bile ducts surrounded by inflammatory cells in a fibrous stroma. This is characteristic in FNH, but not in HCA. According to a meta-analysis, the frequency of central scarring in FNH is 61%;[39] thus, the sensitivity is low. Reflecting the aggregation of vessels and bile ducts, the central scar shows hypointensity on T1WI and hyperintensity on T2WI. Dynamic studies show a progressive contrast effect, reflecting the fibrotic stroma and low signal in the HBP.

- Isointensity or hyperintensity in the HBP

  The hepatocytes present in FNH are functional. Therefore, they take up GA and demonstrate

isointensity or hyperintensity in the HBP versus the surrounding liver. Since most focal liver lesions show hypointensity in the HBP, this finding is useful in differentiating FNH from other hepatic masses. Moreover, since most HCAs also show hypointensity in the HBP, isointensity or hyperintensity during the HBP is reportedly the most useful imaging finding for differentiating FNH from HCA (sensitivity, 0.91–1.00; specificity, 0.87–1.00) (Figure 12).[39–42] However, it has been reported that 14% of HCAs show iso- or hyperintensity in the HBP.[42]

Other Potential or Investigational Applications

Assessment of response after locoregional therapy

JSH guidelines and LI-RADS v2018 advocate the use of dynamic CT and MRI for detecting liver malignancy after locoregional treatment, including transcatheter, locoablative, and external radiation therapies. LI-RADS recommends regular imaging evaluation (i.e., at 1, 3, 6, 9, and 12 months after locoregional therapy, as well as every 3–6 months thereafter). The JSH guidelines suggest conducting dynamic CT or MRI once or twice per year. According to LI-RADS, the criteria used to assess response to treatment for GBCAs and GA are similar.[43] Both CT and MRI can help detect local recurrence based on these criteria. Nevertheless, CT following transcatheter arterial chemoembolization can be problematic due to the high lipiodol content in lesions. MRI is more effective than CT in assessing local recurrence following transcatheter arterial chemoembolization. This is because lipiodol does not show hyperintensity on MRI (Figure 13).[44]

Notably, the JSH guidelines have not discussed the importance of stereotactic body radiation therapy (SBRT) against HCC. The criteria established by the LI-RADS for response to treatment can be utilized following SBRT. Nonetheless, it is important to note that there are SBRT-specific post-treatment changes. APHE (with or without washout) might persist for up to 6 months after SBRT and gradually diminish. The occurrence of persistent APHE shortly after SBRT is not invariably indicative of a persistent tumor, as its size generally decreases over the course of 6–12 months.[45] Following SBRT, the liver parenchyma around the lesion displays temporal alterations on imaging; this phenomenon is termed focal liver response (FLR). FLR presents as a distinct hypointense area in the HBP 1 month after SBRT (Figure 14). Of note, significant correlation exists between the FLR

threshold dose and baseline liver function.[46]

Evaluation of the biliary system

In individuals with normal liver and kidney function, it is estimated that 50% of the GA will be eliminated by the hepatobiliary system, while the other 50% will be eliminated by the kidneys.[47] The biliary system is well depicted in the HBP;[48] thus, the HBP can be useful for the assessment of the biliary system (MR cholangiography). MR cholangiopancreatography (MRCP) is commonly used to evaluate the biliary system; however, MRCP is performed prior to the administration of GA, as GA reduces the signal intensity of the biliary system on MRCP.[49] Previous studies have reported the use of MR cholangiography with GA for evaluating biliary leakage following trauma, transplantation, or surgery.[50–52]

Evaluation of liver fibrosis and function

The function of hepatocytes influences the uptake and excretion of GA; hence, GA-MRI is potentially useful in evaluating liver fibrosis. GA-MRI can be used for the staging of liver fibrosis. However, various methods have been used, such as the relative liver enhancement ratio ($(SI_{HBP}-SI_{pre})/SI_{pre}$), contrast enhancement index (SI_{HBP}/SI_{pre}), liver-to-spleen contrast signal intensity (SI_{HBP}/SI_{spleen}), and increased rates of liver-to-spleen ratio ($(LSR_{HBP}-LSR_{pre})/LSR_{pre}$). SI_{HBP} and SI_{pre} represent the signal intensity of the liver on HBP and pre-contrast images, respectively. SI_{spleen} is the signal intensity of the spleen in the HBP. LSR_{HBP} and LSR_{pre} represent the signal intensity ratio of the liver and spleen on HBP and pre-contrast images, respectively. Measurement of T1 relaxation time may provide useful information for the staging of liver fibrosis.[53] T1 mapping is employed to quantitatively assess the contrast effect by measuring tissue-specific T1 values. In addition, fibrosis and inflammation of the liver may be evaluated without using contrast agents. T1 relaxation time increases owing to an elevation in the extracellular fluid of the liver (a consequence of fibrosis and inflammation).[54] Meta-analyses of the effectiveness of GA-MRI for liver fibrosis staging reported the following pooled sensitivities and specificities (respectively): 0.58–0.77 and 0.82–0.95, (area under the receiver operating characteristic curve [AUROC]: 0.85–0.89) for mild fibrosis ($F\geq1$); 0.57–0.72 and 0.68–0.84

(AUROC: 0.76–0.86) for moderate fibrosis (F≥2); 0.61–0.80 and 0.75–0.91 (AUROC: 0.72–0.94) for severe fibrosis (F≥3); and 0.77–0.86 and 0.77–0.82 (AUROC: 0.88–0.89) for cirrhosis (F4).[55–57]

Moreover, GA-MRI can quantitatively evaluate liver function.[58] Functional liver imaging score (FLIS) is utilized to assess liver function. It is calculated using three imaging features on the HBP, namely liver parenchymal enhancement, biliary contrast excretion, and portal vein signal intensity.[59] Lee et al. revealed that the FLIS was strongly correlated with liver function, and might be utilized for patient stratification into Child–Pugh classes. The optimal FLIS for predicting Child–Pugh class A was ≥5, showing high sensitivity (83.7%) and specificity (94.4%). An FLIS <5 was linked to the occurrence of first hepatic decompensation in Child–Pugh class A patients.[60] Batatis et al. created an algorithm to predict the probability of adverse liver-related outcomes in advanced CLD by combining the FLIS with the splenic craniocaudal diameter. This algorithm can independently predict transplant-free mortality and determine the likelihood of transplant-free survival in patients with advanced CLD.[61]

GA or Extracellular GBCAs?

Although GA is the recommended contrast agent for liver MRI in the majority of cases, GBCAs are occasionally preferable. The Diagnostic Imaging Guideline 2021 established by the Japan Radiological Society states that GBCAs are recommended over GA in the following six scenarios.[62]

1. When the liver function is significantly impaired or in the presence of severe cirrhosis

In case of severe liver dysfunction, there is inadequate enhancement in the HBP due to the reduced uptake of GA.[63,64] Poor uptake of GA by hepatocytes leads to an insufficient signal increase in the liver, thereby reducing the contrast of lesions that do not take up GA. Consequently, this effect reduces the detectability of these lesions. In such patients, dynamic CT or dynamic MRI with GBCAs may yield better results than GA-MRI due to the ineffectiveness of the HBP, which is the primary benefit of GA-MRI (Figure 15). Contrast between the liver and spleen or the liver and intrahepatic vessels may be examined to assess whether the uptake of GA is optimal. A clear high signal in the liver compared with the spleen or intrahepatic vessels is indicative of appropriate uptake. In contrast,

similar signals in the liver and spleen, or the absence of an obvious low signal in the intrahepatic vessels denote poor uptake.[65]

2. When the main purpose is to diagnose hepatic hemangioma

The primary imaging feature of hepatic hemangioma is a prolonged signal increase in the delayed phase. Owing to GA uptake in the surrounding liver parenchyma in the TP, the absence of persistent enhancement of hemangiomas is termed pseudo-washout (Figure 16).[66] Small hemangiomas often exhibit decreased signal intensity and pseudo-washout in the TP. These hemangiomas may resemble small HCCs; however, T2WI and DWI may yield complementary evidence to support the exclusion of small HCCs.[67]

3. When the main purpose is to confirm APHE

The concentration of gadolinium in GA is 0.25 mmol/mL (i.e., half of the concentration included in other GBCAs [0.50 mmol/mL]). In addition, half of the dose of other GBCAs is required for GA (0.20 mL/kg). Therefore, the quantity of gadolinium utilized in a normal-dose GA-MRI is approximately 25% of the amount used in other GBCAs-enhanced MRI (GBCA 0.1 mmol/kg versus GA 0.025 mmol/kg). GA binds weakly and reversibly to plasma proteins (mainly albumin), and its contrast effect in blood is higher than that of GBCAs.[68] These properties compensate, to some extent, for the lower gadollinium dose in GA compared with GBCAs. Nevertheless, the use of GBCAs may be considered when the determination of tumor enhancement in the AP is of particular clinical importance.

4. When specificity is more important than sensitivity in the diagnosis of HCC

Evaluation prior to liver transplantation is applicable. In terms of imaging features, HCC is specifically characterized by an enhancing capsule. On GA-MRI, an enhancing capsule is characterized by ring-like enhancement in the PVP or TP. Nevertheless, recognizing an enhancing capsule in the PVP or TP can be challenging due to the GA uptake by hepatocytes even in the PVP. According to previous studies, enhancing capsules were identified in the PVP using GBCAs and GA

in 23–64%[69–72] and 17–49% of cases,[72–75] respectively.

5. When a transient severe motion (TSM) artifact in the AP is observed with previous GA-MRI

Previous studies showed that a TSM artifact in the AP is more commonly found on GA-MRI versus GBCA-enhanced MRI. This may result in non-diagnostic image quality in the AP (Figure 17).[76] A recent meta-analysis revealed that the pooled incidence of TSM was 13.0% (95% confidence interval: 10.3–16.2%) and 3.2% (1.9–5.2%) in the single and multiple AP study, respectively.[77] The rate of TSM is reportedly higher in studies involving patients from Europe or North America versus those involving patients from Asia or the Pacific (16% vs. 8.8%, respectively).[77] An approach based on deep learning has been published for the automated identification and grading of motion-related artifacts.[78]

6. When examination of abdominal organs and vessels other than the liver is necessary

GBCAs with higher gadolinium concentration are more useful than GA for the three-dimensional reconstruction of arteries and portal veins. In practice, dynamic CT with thin slice images is more commonly performed.

Concerns regarding GA

Scan timing of the AP

Half of the injection volume is used for GA versus GBCAs; this results in a shorter duration, allowing optimal scan timing of the AP. Multiphasic AP imaging may assist in overcoming this problem by providing one or more image sets with minimal artifacts and adequate AP scan timing.[79,80] Free-breathing dynamic MRI with stack-of-stars acquisition can help produce continuous images from the AP to the PVP and TP in a single scan; therefore, the scan timing is not a concern.[81,82] In patients able to hold their breath, free-breathing dynamic MRI with stack-of-stars acquisition may not yield images of higher quality versus breath-holding Cartesian sampling and multiphasic AP imaging. Thus, patients with a history of poor breath-hold with Cartesian sampling and multiphasic AP imaging should undergo free-breathing dynamic MRI with stack-of-stars acquisition.

Longer scan duration and higher cost

Longer scan duration and the higher cost of GA-MRI restrict its utility as a screening method. Abbreviated MRI reduces scan duration by obtaining the minimal imaging sequence required for the evaluation.[83] The entire procedure requires <10 min. Abbreviated MRI with GA (including T2WI, DWI, and the HBP) exhibits the highest effectiveness among abbreviated MRI protocols for focal liver lesion evaluation. This is because DWI and HBP are crucially important for focal liver lesion identification, and T2WI is needed for characterizing focal liver lesions. GA is administered outside the MRI room without dynamic study, thereby minimizing complexity and potentially increasing efficiency. A previous meta-analysis demonstrated that the pooled sensitivity and specificity for HCC detection through abbreviated MRI with GA were 0.86–0.87 and 0.94–0.96, respectively.[84,85] The sensitivity of abbreviated MRI with GA for detecting colorectal liver metastases was 0.93–0.94.[86] Abbreviated MRI with GA may also be beneficial for detecting liver metastases in PDAC.[87] However, its clinical application should be carefully examined, as MRCP cannot be obtained prior to the administration of GA. Another benefit of abbreviated MRI is its cost-effectiveness. According to Canellas et al., the cost of abbreviated MRI with GA was approximately 40% lower than that of full MRI for the monitoring of liver metastasis of colorectal cancer.[86] Consequently, following a thorough investigation of its clinical use, abbreviated MRI with GA might be extensively utilized for HCC or liver metastasis identification.

Adverse events

Hypersensitivity reactions and nephrogenic systemic fibrosis are significant adverse effects of contrast agents used in MRI. A meta-analysis revealed that the rate of hypersensitivity reactions to GA was 0.3% (31/1,4850 cases), without any fatalities. After 6,700,000 administrations of GA, comprising administrations to 106 patients with chronic kidney disease (stages 4–5) or undergoing dialysis, there were no cases of unconfounded nephrogenic systemic fibrosis.[88] Gadolinium retention in the brain is another notable adverse effect of GA. Kanda et al. revealed a correlation between hyperintensity in the globus pallidus and dentate nucleus on T1WI and a prior injection of GBCAs.[89] Even in individuals with normal kidney function, it was found that higher signal intensity in the globus pallidus and

dentate nucleus on unenhanced T1WI is positively correlated with past exposure to linear chelate GBCAs; however, this correlation was not observed after exposure to macrocyclic chelate GBCAs.[90] Therefore, gadolinium retention in the body is higher after exposure to linear chelate GBCAs versus macrocyclic chelate GBCAs. GA is a linear chelate contrast agent; nevertheless, it is more thermodynamically stable than other agents of this type.[91] In addition, as previously mentioned, the amount of gadolinium used in normal-dose GA-MRI is markedly lower than that employed in other GBCA-enhanced MRI examinations. Thus, GA is associated with a lower likelihood of retention in the brain compared with other linear GBCAs.[92]

Conclusion

In this review article, we described the fundamentals of GA-MRI, which is a crucial method for liver examination in the clinical setting. GA-MRI is a thorough diagnostic technique that helps to effectively and rapidly assess focal liver lesions and CLD. Nevertheless, GA-MRI is characterized by drawbacks, which include TSM and longer scan durations. GA-MRI cannot be applied to all patients. Therefore, it is essential to comprehend its properties and utilize it in patients with appropriate indications.

Conflicts of Interest

The authors do not have conflicts of interest to declare.

References

1. Paik JM, Golabi P, Younossi Y, et al. Changes in the Global Burden of Chronic Liver Diseases From 2012 to 2017: The Growing Impact of NAFLD. *Hepatology*. 2020;72(5):1605–1616.

2. Toh MR, Wong Yi Ting E, Wong Hei S, et al. Global epidemiology and genetics of hepatocellular carcinoma. *Gastroenterology*. 2023;S0016-5085(23)00105-1..

3. Murakami T, Sofue K, Hori M. Diagnosis of Hepatocellular Carcinoma Using Gd-EOB-DTPA MR Imaging. *Magn Reson Med Sci.* 2022;21(1):168–181.

4. Ichikawa S, Goshima S. Clinical Significance of Liver MR Imaging. *Magn. Reson. Med. Sci.* 2023;22(2):157–175.

5. CT/MRI LI-RADS® v2018. Available at: https://www.acr.org/Clinical-Resources/Reporting-and-Data-Systems/LI-RADS/LI-RADS-CT-MRI-v2018.

6. Ito K, Mitchell DG, Outwater EK, et al. Hepatic lesions: discrimination of nonsolid, benign lesions from solid, malignant lesions with heavily T2-weighted fast spin-echo MR imaging. *Radiology*. 1997;204(3):729–737.

7. Kim YK, Kwak HS, Kim CS, et al. Detection and characterization of focal hepatic tumors: a comparison of T2-weighted MR images before and after the administration of gadoxectic acid. *J Magn Reson Imaging*. 2009;30(2):437–443.

8. Kitao A, Matsui O, Yoneda N, et al. Gadoxetic acid-enhanced MR imaging for hepatocellular carcinoma: molecular and genetic background. *Eur Radiol.* 2020;30(6):3438–3447.

9. Liu X, Jiang H, Chen J, et al. Gadoxetic acid disodium-enhanced magnetic resonance imaging outperformed multidetector computed tomography in diagnosing small hepatocellular carcinoma: A meta-analysis. *Liver Transpl.* 2017;23(12):1505–1518.

10. Guo J, Seo Y, Ren S, et al. Diagnostic performance of contrast-enhanced multidetector computed tomography and gadoxetic acid disodium-enhanced magnetic resonance imaging in detecting hepatocellular carcinoma: direct comparison and a meta-analysis. *Abdom Radiol (NY).* 2016;41(10):1960–1972.

11. Liu X, Zou L, Liu F, et al. Gadoxetic acid disodium-enhanced magnetic resonance imaging for the detection of hepatocellular carcinoma: a meta-analysis. *PLoS One*. 2013;8(8):e70896.

12. Wang J, Ye X, Li J, et al. The diagnostic performance of gadoxetic acid disodium-enhanced magnetic resonance imaging and contrast-enhanced ultrasound in detecting hepatocellular carcinoma: A meta-analysis. *Medicine*. 2021;100(6):e24602.

13. Junqiang L, Yinzhong W, Li Z, et al. Gadoxetic acid disodium (Gd-EOBDTPA)-enhanced magnetic resonance imaging for the detection of hepatocellular carcinoma: a meta-analysis. *J Magn Reson Imaging*. 2014;39(5):1079–1087.

14. Yinzhong W, Xiaoxue T, Jinhui T, et al. Is Gadoxetic Acid Disodium (Gd-EOB-DTPA)-Enhanced Magnetic Resonance Imaging an Accurate Diagnostic Method for Hepatocellular Carcinoma? A Systematic Review with Meta-Analysis. *Curr Med Imaging Rev*. 2022;18(6):633–647.

15. Li X, Li C, Wang R, et al. Combined Application of Gadoxetic Acid Disodium-Enhanced Magnetic Resonance Imaging (MRI) and Diffusion-Weighted Imaging (DWI) in the Diagnosis of Chronic Liver Disease-Induced Hepatocellular Carcinoma: A Meta-Analysis. *PLoS One*. 2015;10(12):e0144247.

16. Ye F, Liu J, Ouyang H. Gadolinium Ethoxybenzyl Diethylenetriamine Pentaacetic Acid (Gd-EOB-DTPA)-Enhanced Magnetic Resonance Imaging and Multidetector-Row Computed Tomography for the Diagnosis of Hepatocellular Carcinoma: A Systematic Review and Meta-analysis. *Medicine*. 2015;94(32):e1157.

17. Duncan JK, Ma N, Vreugdenburg TD, et al. Gadoxetic acid-enhanced MRI for the characterization of hepatocellular carcinoma: A systematic review and meta-analysis. *J Magn Reson Imaging*. 2017;45(1):281–290.

18. Ricke J, Steffen IG, Bargellini I, et al. Gadoxetic acid-based hepatobiliary MRI in hepatocellular carcinoma. *JHEP Rep.* 2020;2(6):100173.

19. Wu Y, Zhu M, Liu Y, et al. Peritumoral Imaging Manifestations on Gd-EOB-DTPA-Enhanced MRI for Preoperative Prediction of Microvascular Invasion in Hepatocellular Carcinoma: A Systematic Review and Meta-Analysis. *Front Oncol.* 2022;12:907076.

20. Kudo M, Kawamura Y, Hasegawa K, et al. Management of Hepatocellular Carcinoma in Japan: JSH Consensus Statements and Recommendations 2021 Update. *Liver Cancer*. 2021;10(3):181–223.

21. Nishie A, Goshima S, Haradome H, et al. Cost-effectiveness of EOB-MRI for Hepatocellular Carcinoma in Japan. *Clin Ther.* 2017;39(4):738-750.e4.

22. Motosugi U, Murakami T, Lee JM, et al. Recommendation for terminology: Nodules without arterial phase hyperenhancement and with hepatobiliary phase hypointensity in chronic liver disease. *J Magn Reson Imaging*. 2018;48(5):1169–1171.

23. Suh CH, Kim KW, Pyo J, et al. Hypervascular Transformation of Hypovascular Hypointense Nodules in the Hepatobiliary Phase of Gadoxetic Acid-Enhanced MRI: A Systematic Review and Meta-Analysis. *AJR Am J Roentgenol.* 2017;209(4):781–789.

24. Kim T-H, Woo S, Han S, et al. Risk Factors for Hypervascularization in Hepatobiliary Phase Hypointense Nodules without Arterial Phase Hyperenhancement: A Systematic Review and Meta-analysis. *Acad Radiol.* 2022;29(2):198–210.

25. Joo I, Kim SY, Kang TW, et al. Radiologic-Pathologic Correlation of Hepatobiliary Phase Hypointense Nodules without Arterial Phase Hyperenhancement at Gadoxetic Acid-enhanced MRI: A Multicenter Study. *Radiology*. 2020;296(2):335–345.

26. Matsuda M, Ichikawa S, Matsuda M, et al. Hepatobiliary phase hypointense nodule without arterial phase hyperenhancement as a risk factor for late recurrence (>1 year) of hepatocellular carcinoma after surgery. *Clin Radiol.* 2019;74(12):975.e1-975.e9.

27. Cha DI, Jang KM, Kim SH, et al. Preoperative Prediction for Early Recurrence Can Be as Accurate as Postoperative Assessment in Single Hepatocellular Carcinoma Patients. *Korean J Radiol.* 2020;21(4):402–412.

28. Kim T-H, Woo S, Han S, et al. Hepatobiliary phase hypointense nodule without arterial phase hyperenhancement: are they at risk of HCC recurrence after ablation or surgery? A systematic review and meta-analysis. *Eur Radiol.* 2020;30(3):1624–1633.

29. Ichikawa S, Ichikawa T, Motosugi U, et al. Was Hypervascular Hepatocellular Carcinoma Visible on Previous Gadoxetic Acid-Enhanced Magnetic Resonance Images? *Liver Cancer*. 2015;4(3):154–162.

30. Ichikawa S, Ichikawa T, Motosugi U, et al. Presence of a hypovascular hepatic nodule showing hypointensity on hepatocyte-phase image is a risk factor for hypervascular hepatocellular carcinoma. *J Magn Reson Imaging*. 2014;39(2):293–297.

31. Shimizu T, Motosugi U, Komatsu N, et al. MRI-based risk factors of hepatocellular carcinoma in patients with chronic liver disease: A prospective observational study. *J Magn Reson Imaging*. 2020;51(2):389–396.

32. Choi SH, Kim SY, Park SH, et al. Diagnostic performance of CT, gadoxetate disodium-enhanced MRI, and PET/CT for the diagnosis of colorectal liver metastasis: Systematic review and meta-analysis. *J Magn Reson Imaging*. 2018;47(5):1237–1250.

33. Sofue K, Tsurusaki M, Murakami T, et al. Does Gadoxetic acid-enhanced 3.0T MRI in addition to 64-detector-row contrast-enhanced CT provide better diagnostic performance and change the therapeutic strategy for the preoperative evaluation of colorectal liver metastases? *Eur Radiol.* 2014;24(10):2532–2539.

34. Vilgrain V, Esvan M, Ronot M, et al. A meta-analysis of diffusion-weighted and gadoxetic acid-enhanced MR imaging for the detection of liver metastases. *Eur Radiol.* 2016;26(12):4595–4615.

35. Zech CJ, Korpraphong P, Huppertz A, et al. Randomized multicentre trial of gadoxetic acid-enhanced MRI versus conventional MRI or CT in the staging of colorectal cancer liver metastases. *Br J Surg.* 2014;101(6):613–621.

36. Zech CJ, Justo N, Lang A, et al. Cost evaluation of gadoxetic acid-enhanced magnetic resonance imaging in the diagnosis of colorectal-cancer metastasis in the liver: Results from the VALUE Trial. *Eur Radiol.* 2016;26(11):4121–4130.

37. Motosugi U, Ichikawa T, Morisaka H, et al. Detection of pancreatic carcinoma and liver metastases with gadoxetic acid-enhanced MR imaging: comparison with contrast-enhanced multi-detector row CT. *Radiology*. 2011;260(2):446–453.

38. Ichikawa S, Morisaka H, Omiya Y, et al. Distinction Between Hepatocellular Carcinoma and Hypervascular Liver Metastases in Non-cirrhotic Patients Using Gadoxetate Disodium-Enhanced Magnetic Resonance Imaging. *Can Assoc Radiol J.* 2022;73(4):639–646.

39. Suh CH, Kim KW, Kim GY, et al. The diagnostic value of Gd-EOB-DTPA-MRI for the diagnosis of focal nodular hyperplasia: a systematic review and meta-analysis. *Eur Radiol.* 2015;25(4):950–960.

40. McInnes MDF, Hibbert RM, Inácio JR, et al. Focal Nodular Hyperplasia and Hepatocellular Adenoma: Accuracy of Gadoxetic Acid-enhanced MR Imaging--A Systematic Review. *Radiology*. 2015;277(2):413–423.

41. Guo Y, Li W, Cai W, et al. Diagnostic Value of Gadoxetic Acid-Enhanced MR Imaging to Distinguish HCA and Its Subtype from FNH: A Systematic Review. *Int J Med Sci.* 2017;14(7):668–674.

42. Kim T-H, Woo S, Ebrahimzadeh S, et al. Hepatic Adenoma Subtypes on Hepatobiliary Phase of Gadoxetic Acid-Enhanced MRI: Systematic Review and Meta-Analysis. *AJR Am J Roentgenol.* 2023;220(1):28–38.

43. Kim T-H, Woo S, Joo I, et al. LI-RADS treatment response algorithm for detecting incomplete necrosis in hepatocellular carcinoma after locoregional treatment: a systematic review and meta-analysis using individual patient data. *Abdom Radiol (NY)*. 2021;46(8):3717–3728.

44. Tsujita Y, Sofue K, Ueshima E, et al. Evaluation and Prediction of Treatment Response for Hepatocellular Carcinoma. *Magn Reson Med Sci*. 2023;22(2):209–220.

45. Alnammi M, Wortman J, Therrien J, et al. MRI features of treated hepatocellular carcinoma following locoregional therapy: a pictorial review. *Abdom Radiol (NY)*. 2022;47(7):2299–2313.

46. Sanuki N, Takeda A, Oku Y, et al. Threshold doses for focal liver reaction after stereotactic ablative body radiation therapy for small hepatocellular carcinoma depend on liver function: evaluation on magnetic resonance imaging with Gd-EOB-DTPA. *Int J Radiat Oncol Biol Phys.* 2014;88(2):306–311.

47. Hamm B, Staks T, Mühler A, et al. Phase I clinical evaluation of Gd-EOB-DTPA as a hepatobiliary MR contrast agent: safety, pharmacokinetics, and MR imaging. *Radiology*. 1995;195(3):785–792.

48. Ihara K, Onoda H, Tanabe M, et al. Breath-hold High-resolution T1-weighted Gradient Echo Liver MR Imaging with Compressed Sensing Obtained during the Gadoxetic Acid-enhanced

Hepatobiliary Phase: Image Quality and Lesion Visibility Compared with a Standard T1-weighted Sequence. *Magn Reson Med Sci.* 2023. Available at: http://dx.doi.org/10.2463/mrms.mp.2022-0137.

49. Nakamura Y, Ohmoto T, Saito T, et al. Effects of gadolinium-ethoxybenzyl-diethylenetriamine pentaacetic acid on T2-weighted MRCP. *Magn Reson Med Sci.* 2009;8(4):143–148.
50. Wong Y-C, Wang L-J, Wu C-H, et al. Detection and characterization of traumatic bile leaks using Gd-EOB-DTPA enhanced magnetic resonance cholangiography. *Sci Rep.* 2018;8(1):14612.
51. Lim CJ, Hong K, Lee J-M, et al. Clinical usefulness of T1-weighted MR cholangiography with Gd-EOB-DTPA for the evaluation of biliary complication after liver transplantation. *Ann Hepatobiliary Pancreat Surg*. 2021;25(1):39–45.
52. Petrillo M, Ierardi AM, Tofanelli L, et al. Gd-EOB-DTP-enhanced MRC in the preoperative percutaneous management of intra and extrahepatic biliary leakages: does it matter? *Gland Surg*. 2019;8(2):174–183.
53. Sheng RF, Wang HQ, Yang L, et al. Assessment of liver fibrosis using T1 mapping on Gd-EOB-DTPA-enhanced magnetic resonance. *Dig Liver Dis.* 2017;49(7):789–795.
54. Schaapman JJ, Tushuizen ME, Coenraad MJ, et al. Multiparametric MRI in Patients With Nonalcoholic Fatty Liver Disease. *J Magn Reson Imaging*. 2021;53(6):1623–1631.
55. Lai L-Y, Huang M-P, Su S, et al. Liver Fibrosis Staging with Gadolinium Ethoxybenzyl Diethylenetriamine Penta-Acetic Acid-enhanced: A Systematic Review and Meta-analysis. *Curr Med Imaging Rev.* 2021;17(7):854–863.
56. Yang D, Li D, Li J, et al. Systematic review: The diagnostic efficacy of gadoxetic acid-enhanced MRI for liver fibrosis staging. *Eur J Radiol.* 2020;125:108857.
57. Li X, Liu H, Wang R, et al. Gadoxetate-disodium-enhanced magnetic resonance imaging for liver fibrosis staging: a systematic review and meta-analysis. *Clin Radiol.* 2020;75(4):319.e11-319.e19.
58. Poetter-Lang S, Bastati N, Messner A, et al. Quantification of liver function using gadoxetic acid-enhanced MRI. *Abdom Radiol (NY).* 2020;45(11):3532–3544.

59. Bastati N, Wibmer A, Tamandl D, et al. Assessment of Orthotopic Liver Transplant Graft Survival on Gadoxetic Acid-Enhanced Magnetic Resonance Imaging Using Qualitative and Quantitative Parameters. *Invest Radiol.* 2016;51(11):728–734.

60. Lee HJ, Hong SB, Lee NK, et al. Validation of functional liver imaging scores (FLIS) derived from gadoxetic acid-enhanced MRI in patients with chronic liver disease and liver cirrhosis: the relationship between Child-Pugh score and FLIS. *Eur Radiol.* 2021;31(11):8606–8614.

61. Bastati N, Beer L, Ba-Ssalamah A, et al. Gadoxetic acid-enhanced MRI-derived functional liver imaging score (FLIS) and spleen diameter predict outcomes in ACLD. *J Hepatol.* 2022;77(4):1005–1013.

62. Japan Radiological Society ed. *Diagnostic Imaging Guideline 2021*. Tokyo: KANEHARA & Co., LTD.; 2021.

63. Ko JS, Byun J, Park S, et al. Prediction of insufficient hepatic enhancement during the Hepatobiliary phase of Gd-EOB DTPA-enhanced MRI using machine learning classifier and feature selection algorithms. *Abdom Radiol (NY)*. 2022;47(1):161–173.

64. Mori Y, Motosugi U, Shimizu T, et al. Predicting Patients With Insufficient Liver Enhancement in the Hepatobiliary Phase Before the Injection of Gadoxetic Acid: A Practical Approach Using the Bayesian Method. *J Magn Reson Imaging*. 2020;51(1):62–69.

65. Yang M, Zhang Y, Zhao W, et al. Evaluation of liver function using liver parenchyma, spleen and portal vein signal intensities during the hepatobiliary phase in Gd-EOB-D TPA-enhanced MRI. *BMC Med Imaging*. 2020;20(1):119.

66. Tateyama A, Fukukura Y, Takumi K, et al. Hepatic Hemangiomas: Factors Associated with Pseudo Washout Sign on Gd-EOB-DTPA-enhanced MR Imaging. *Magn Reson Med Sci.* 2016;15(1):73–82.

67. Nam SJ, Yu J-S, Cho E-S, et al. High-flow haemangiomas versus hypervascular hepatocellular carcinoma showing “pseudo-washout” on gadoxetic acid-enhanced hepatic MRI: value of diffusion-weighted imaging in the differential diagnosis of small lesions. *Clin Radiol.* 2017;72(3):247–254.

68. Cavagna FM, Maggioni F, Castelli PM, et al. Gadolinium chelates with weak binding to serum proteins. A new class of high-efficiency, general purpose contrast agents for magnetic resonance imaging. *Invest Radiol.* 1997;32(12):780–796.

69. Rimola J, Forner A, Tremosini S, et al. Non-invasive diagnosis of hepatocellular carcinoma ≤ 2 cm in cirrhosis. Diagnostic accuracy assessing fat, capsule and signal intensity at dynamic MRI. *J Hepatol.* 2012;56(6):1317–1323.

70. Khan AS, Hussain HK, Johnson TD, et al. Value of delayed hypointensity and delayed enhancing rim in magnetic resonance imaging diagnosis of small hepatocellular carcinoma in the cirrhotic liver. *J Magn Reson Imaging*. 2010;32(2):360–366.

71. Ishigami K, Yoshimitsu K, Nishihara Y, et al. Hepatocellular carcinoma with a pseudocapsule on gadolinium-enhanced MR images: correlation with histopathologic findings. *Radiology*. 2009;250(2):435–443.

72. Schelhorn J, Best J, Dechêne A, et al. Evaluation of combined Gd-EOB-DTPA and gadobutrol magnetic resonance imaging for the prediction of hepatocellular carcinoma grading. *Acta radiol.* 2016;57(8):932–938.

73. Ichikawa S, Motosugi U, Oishi N, et al. Ring-Like Enhancement of Hepatocellular Carcinoma in Gadoxetic Acid-Enhanced Multiphasic Hepatic Arterial Phase Imaging With Differential Subsampling With Cartesian Ordering. *Invest Radiol.* 2018;53(4):191–199.

74. Kim Y, Furlan A, Borhani AA, et al. Computer-aided diagnosis program for classifying the risk of hepatocellular carcinoma on MR images following liver imaging reporting and data system (LI-RADS). *J Magn Reson Imaging*. 2018;47(3):710–722.

75. Joo I, Lee JM, Lee DH, et al. Liver imaging reporting and data system v2014 categorization of hepatocellular carcinoma on gadoxetic acid-enhanced MRI: Comparison with multiphasic multidetector computed tomography. *J Magn Reson Imaging*. 2017;45(3):731–740.

76. Tanabe M, Higashi M, Iida E, et al. Transient respiratory motion artifacts in multiple arterial phases on abdominal dynamic magnetic resonance imaging: a comparison using gadoxetate disodium and gadobutrol. *Jpn J Radiol.* 2021;39(2):178–185.

77. Kim DW, Choi SH, Park T, et al. Transient Severe Motion Artifact on Arterial Phase in Gadoxetic Acid-Enhanced Liver Magnetic Resonance Imaging: A Systematic Review and Meta-analysis. *Invest Radiol.* 2022;57(1):62–70.

78. Park T, Kim DW, Choi SH, et al. Deep Learning-Based Automatic Detection and Grading of Motion-Related Artifacts on Gadoxetic Acid-Enhanced Liver MRI. *Invest Radiol.* 2023;58(2):166–172.

79. Ichikawa S, Motosugi U, Sato K, et al. Transient Respiratory-motion Artifact and Scan Timing during the Arterial Phase of Gadoxetate Disodium-enhanced MR Imaging: The Benefit of Shortened Acquisition and Multiple Arterial Phase Acquisition. *Magn Reson Med Sci.* 2021;20(3):280–289.

80. Kim JH, Yoon JH, Bae JS, et al. Multiarterial Phase Acquisition in Gadoxetic Acid-Enhanced Liver MRI for the Detection of Hypervascular Hepatocellular Carcinoma in High-Risk Patients: Comparison of Compressed Sensing Versus View Sharing Techniques. *Invest Radiol.* 2023;58(2):139–147.

81. Endler CH-J, Kukuk GM, Peeters JM, et al. Dynamic Liver Magnetic Resonance Imaging During Free Breathing: A Feasibility Study With a Motion Compensated Variable Density Radial Acquisition and a Viewsharing High-Pass Filtering Reconstruction. *Invest Radiol.* 2022;57(7):470–477.

82. Ichikawa S, Motosugi U, Wakayama T, et al. An Intra-individual Comparison between Free-breathing Dynamic MR Imaging of the Liver Using Stack-of-stars Acquisition and the Breath-holding Method Using Cartesian Sampling or View-sharing. *Magn. Reson. Med. Sci.* 2023;22(2):221–231.

83. Altinmakas E, Taouli B. Abbreviated Liver Magnetic Resonance Imaging Protocols and Applications. *Radiol Clin North Am.* 2022;60(5):695–703.

84. Gupta P, Soundararajan R, Patel A, et al. Abbreviated MRI for hepatocellular carcinoma screening: A systematic review and meta-analysis. *J Hepatol.* 2021;75(1):108–119.

85. Kim DH, Choi SH, Shim JH, et al. Meta-Analysis of the Accuracy of Abbreviated Magnetic Resonance Imaging for Hepatocellular Carcinoma Surveillance: Non-Contrast versus Hepatobiliary Phase-Abbreviated Magnetic Resonance Imaging. *Cancers*. 2021;13(12):2975.

86. Canellas R, Patel MJ, Agarwal S, et al. Lesion detection performance of an abbreviated gadoxetic acid-enhanced MRI protocol for colorectal liver metastasis surveillance. *Eur Radiol.* 2019;29(11):5852–5860.

87. Yamaguchi T, Sofue K, Ueshima E, et al. Abbreviated Gadoxetic Acid-Enhanced MRI for the Detection of Liver Metastases in Patients With Potentially Resectable Pancreatic Ductal Adenocarcinoma. *J Magn Reson Imaging*. 2022;56(3):725–736.

88. Schieda N, van der Pol CB, Walker D, et al. Adverse Events to the Gadolinium-based Contrast Agent Gadoxetic Acid: Systematic Review and Meta-Analysis. *Radiology*. 2020;297(3):565–572.

89. Kanda T, Ishii K, Kawaguchi H, et al. High signal intensity in the dentate nucleus and globus pallidus on unenhanced T1-weighted MR images: relationship with increasing cumulative dose of a gadolinium-based contrast material. *Radiology*. 2014;270(3):834–841.

90. Kanda T, Osawa M, Oba H, et al. High Signal Intensity in Dentate Nucleus on Unenhanced T1-weighted MR Images: Association with Linear versus Macrocyclic Gadolinium Chelate Administration. *Radiology*. 2015;275(3):803–809.

91. Schmitt-Willich H, Brehm M, Ewers CLJ, et al. Synthesis and Physicochemical Characterization of a New Gadolinium Chelate: The Liver-Specific Magnetic Resonance Imaging Contrast Agent Gd-EOB-DTPA. *Inorg Chem.* 1999;38(6):1134–1144.

92. Ichikawa S, Motosugi U, Omiya Y, et al. Contrast Agent-Induced High Signal Intensity in Dentate Nucleus on Unenhanced T1-Weighted Images: Comparison of Gadodiamide and Gadoxetic Acid. *Invest Radiol.* 2017;52(7):389–395.

Figure Legends

Figure 1. Scan timing of the arterial phase.

(A) Premature (69-year-old male patient): enhancement of the hepatic artery (arrow), but no or weak enhancement of the portal vein (arrowhead).

(B) Optimal (59-year-old female patient): enhancement of the hepatic artery (arrow) and portal vein (arrowhead), but no enhancement of the hepatic vein (open arrow) on antegrade flow.

(C) Delayed (73-year-old female patient): enhancement of the hepatic vein (open arrow).

Figure 2. Multiple focal liver lesions in a 62-year-old female patient with a history of distal pancreatectomy for insulinoma.

(A, B) Diffusion-weighted images (DWI) revealing three hyperintense lesions in the liver metastasis (9 mm in diameter), arrow; hemangioma (22 mm in diameter), arrowhead; cyst (13 mm in diameter), open arrow). It was difficult to distinguish between the lesions based on DWI signals alone. Liver metastasis showing a lower signal than the cyst and hemangioma on fat-saturated T2-weighted images (T2WI) (C, D) and heavily T2WI at echo time 150 ms (E, F). Hemangioma showing a slightly lower signal than the cyst in the heavily T2WI (E, F).

Figure 3. Hepatocellular carcinoma in a 75-year-old male patient with chronic hepatitis caused by infection with hepatitis C virus.

(A) Pre-contrast and (B) arterial-phase gadoxetic acid-enhanced magnetic resonance imaging revealing a hypervascular nodule in segment 6 of the liver (arrows). (C) The nodule (15 mm in diameter) showing washout in the portal venous phase and hypointensity in the (D) traditional and (E) hepatobiliary phases. An enhancing capsule was observed in the portal venous and traditional phases. Nodule showing signal reduction between the (F) in-phase and (G) opposed-phase images, revealing intratumoral fat. Nodule showing moderate hyperintensity in the (H) T2-weighted image and diffusion restriction in the (I) diffusion-weighted image. It was scored LR-5 according to the Liver Imaging Reporting and Data System version 2018, and identified as hepatocellular carcinoma.

Figure 4. Hepatocellular carcinomas in an 86-year-old male patient with liver cirrhosis caused by infection with hepatitis C virus.

(A) Pre-contrast and (B) arterial phase gadoxetic acid-enhanced magnetic resonance imaging revealing a hypervascular nodule in segment 3 of the liver (arrows). (C) Nodule showing partial washout and an enhancing capsule in the portal venous phase, measuring 25 mm in diameter (arrow). (D) The area without washout showing hyperintensity in the hepatobiliary phase due to the uptake of gadoxetic acid (arrowhead).

Figure 5. Hepatocellular carcinomas in a 79-year-old male patient with liver cirrhosis caused by infection with hepatitis C virus.

(A) Arterial and (B) delayed phase contrast-enhanced computed tomography revealing no focal liver lesions (dotted circles). (C) Arterial phase and (D) hepatobiliary phase gadoxetic acid-enhanced magnetic resonance imaging, performed 2 weeks later, revealing hypervascular nodules with hypointensity in the hepatobiliary phase in segment 3 of the liver. These nodules measured 13 mm (arrows) and 8 mm (arrowheads) in diameter.

Figure 6. Hepatocellular carcinoma with microvascular invasion in a 72-year-old male patient with liver cirrhosis caused by alcoholic hepatitis.

(A) Arterial and (B) hepatobiliary phase gadoxetic acid-enhanced magnetic resonance imaging revealing a hepatocellular carcinoma (arrows) with peritumoral arterial enhancement and peritumoral hypointensity (arrowheads). (C) Hematoxylin-and-eosin staining (×400) of the surgical specimen confirming microvascular invasion (open arrows).

Figure 7. Hepatocellular carcinoma in a 73-year-old male patient with liver cirrhosis caused by infection with hepatitis B virus.

(A) Arterial phase and (B) hepatobiliary phase (HBP) gadoxetic acid-enhanced magnetic resonance imaging (MRI) revealing an HBP hypointense nodule without arterial phase hyperenhancement measuring 13 mm in diameter (solid and dotted arrows), in segment 3 of the liver on the baseline MRI.

(C, D) The size of this nodule did not change, but showed an intratumoral hypervascular focus measuring 7 mm in diameter (arrowhead) on follow-up MRI.

Figure 8. Hepatocellular carcinoma in a 77-year-old male patient with liver cirrhosis caused by infection with hepatitis B virus.
(A) Arterial phase and (B) hepatobiliary phase (HBP) gadoxetic acid-enhanced magnetic resonance imaging (MRI) revealing an HBP hypointense nodule without arterial phase hyperenhancement measuring 8 mm in diameter (solid and dotted arrows), in segment 7 of the liver on the baseline MRI. (C, D) This nodule did not change in size and did not show hypervascularity in the arterial phase on follow-up MRI (solid and dotted arrows). Another hypointense nodule measuring 10 mm in diameter was visible in segment 7, with hypervascularity (arrowheads). It was not possible to detect this nodule on the baseline MRI (dotted circles).

Figure 9. Colorectal liver metastases in a 76-year-old female patient without chronic liver diseases.
(A) Arterial phase and (B) delayed phase contrast-enhanced computed tomography (CT) revealing a hypoattenuating nodule measuring 10 mm in segment 8 of the liver (arrows). This nodule showed hyperintensity on (C) diffusion-weighted imaging and hypointensity in the (D) hepatobiliary phase during gadoxetic acid-enhanced magnetic resonance imaging (MRI) performed 1 week after CT (arrows). Other small nodules were detected via gadoxetic acid-enhanced MRI in segments 4 and 3 of the liver (open arrows and arrowheads). These small nodules were not be detected by CT (dotted circles).

Figure 10. Liver metastasis from pancreatic ductal adenocarcinoma in an 82-year-old male patient without chronic liver diseases.
(A) Arterial phase gadoxetic acid-enhanced magnetic resonance imaging revealing a wedge-shaped hyperenhanced area in segment 8 of the liver. This could be misdiagnosed as an arterioportal shunt (arrow). Nodule showing slight hypointensity in the (B) portal venous phase (arrowhead). Hepatobiliary phase imaging clearly showing a hypointense nodule measuring 7 mm, which clearly

shows hyperintensity on the diffusion-weighted image (arrows).

Figure 11. Hypervascular liver metastasis from pancreatic neuroendocrine carcinoma in a 36-year-old female patient without chronic liver diseases.
(A) Pre-contrast and (B) arterial phase gadoxetic acid-enhanced magnetic resonance imaging revealing a hypervascular nodule measuring 10 mm in segment 8 of the liver (arrow). Nodule showing no washout in the (C) portal venous phase and hypointensity with rim hyperintensity in the (D) hepatobiliary phase.

Figure 12. Comparison of hepatocellular adenoma (HCA) and focal nodular hyperplasia (FNH)
Upper row: HCA in a 28-year-old female patient without chronic liver diseases.
Lower row: FNH in a 36-year-old female patient without chronic liver diseases.
(A) Arterial phase gadoxetic acid-enhanced magnetic resonance imaging (MRI) revealing a hypervascular nodule measuring 27 mm in segment 7 of the liver (arrow). Nodule showing hypointensity in the (B) hepatobiliary phase (HBP), which is a typical imaging finding of HCA.
(C) Arterial phase gadoxetic acid-enhanced MRI revealing a hypervascular nodule measuring 30 mm in segment 7 of the liver (arrowhead). Nodule showing hyperintensity in the (D) HBP, which is a typical imaging finding of FNH.

Figure 13. Recurrent hepatocellular carcinoma after transcatheter arterial chemoembolization in a 62-year-old male patient with liver cirrhosis caused by nonalcoholic steatohepatitis.
(A) Pre-contrast computed tomography (CT) performed 15 months after transcatheter arterial chemoembolization revealing lipiodol accumulation in segment 8 of the liver (arrow). (B) Arterial phase (AP) and (C) portal venous phase (PVP) contrast CT revealing a focal defect of lipiodol accumulation (arrowhead). Nodular enhancement and washout are present (dotted arrow); however, the detection of nodular enhancement on CT was challenging owing to the high accumulation of lipiodol in the lesion. Lipiodol accumulation not showing high signal intensity on (D) pre-contrast magnetic resonance imaging (MRI); thus, the nodular enhancement can be clearly detected in the (E)

AP contrast-enhanced MRI (arrowhead). (F) PVP contrast-enhanced MRI clearly revealing washout (arrowhead).

Figure 14. Stereotactic body radiation therapy (SBRT) for recurrent hepatocellular carcinoma after radiofrequency ablation in an 88-year-old female patient with liver cirrhosis caused by infection with hepatitis C virus.

(A) Arterial phase (AP) and (B) portal venous phase (PVP) contrast-enhanced magnetic resonance imaging (MRI) revealing a nodule measuring 20 mm in diameter and displaying AP hyperenhancement and washout (arrows) near the post-ablation area (dotted arrows). (C) Nodule clearly showing hypointensity in the hepatobiliary phase. (D) AP and (E) PVP contrast-enhanced MRI performed 5 months after SBRT (48 Gy in four fractions), revealing a decrease in nodular size and no AP hyperenhancement (arrowheads). The lesion met the non-viable criteria stated in the Liver Imaging Reporting and Data System version 2018. Liver parenchyma around the target lesion showing AP hyperenhancement and persistent enhancement on the PVP (open arrows). This region is shown as a distinct area of low signal intensity in the hepatobiliary phase (open arrows).

Figure 15. Hepatocellular carcinomas in a 68-year-old male patient with liver cirrhosis caused by alcoholic hepatitis.

(A) Arterial phase and (B) portal venous phase contrast-enhanced computed tomography revealing a hypervascular nodule measuring 12 mm in diameter, with a washout appearance, in segment 8 of the liver (arrows). (C) Arterial phase gadoxetic acid-enhanced magnetic resonance imaging also revealing the hypervascular nodule (arrow); this nodule showed isointensity compared with the intensity displayed by the surrounding liver parenchyma in the (D) hepatobiliary phase (dotted arrow). In patients with severely impaired liver function, the liver parenchyma shows a comparable signal to that of intrahepatic vessels due to the decreased uptake of gadoxetic acid.

Figure 16. Hepatic hemangiomas in a 50-year-old female patient without chronic liver diseases.

(A) Pre-contrast and (B) arterial phase gadoxetic acid-enhanced magnetic resonance imaging revealing

a partially enhancing nodule measuring 15 mm in diameter in segment 7 of the liver (arrows). Nodule showing centripetal enhancement in the (C) portal venous phase. This finding is compatible with a cavernous hemangioma; however, this nodule shows hypointensity compared with the intensity displayed by the surrounding liver parenchyma (pseudo-washout) in the (D) transitional phase (arrowhead).

Figure 17. Examples of transient severe motion in a 79-year-old female patient without chronic liver diseases.

Upper row: Dynamic magnetic resonance imaging (MRI) using gadoxetic acid (GA).

Lower row: Dynamic MRI using an extracellular gadolinium-based contrast agent (GBCA), performed 1 year before GA-enhanced MRI.

(A) Pre-contrast MRI showing good breath-holding. Following the injection of GA, breath-holding is poor in the (B) arterial phase (AP) only (arrows), with good breath-holding observed in the (C) portal venous and (D) transitional phases. Dynamic MRI with GBCA showing good breath-holding in all phases, including AP, i.e., (E) pre-contrast, (F) AP, (G) portal venous phase, and (H) equilibrium phase.

Figure 1

Click here to access/download;Figure;Figure1.tif

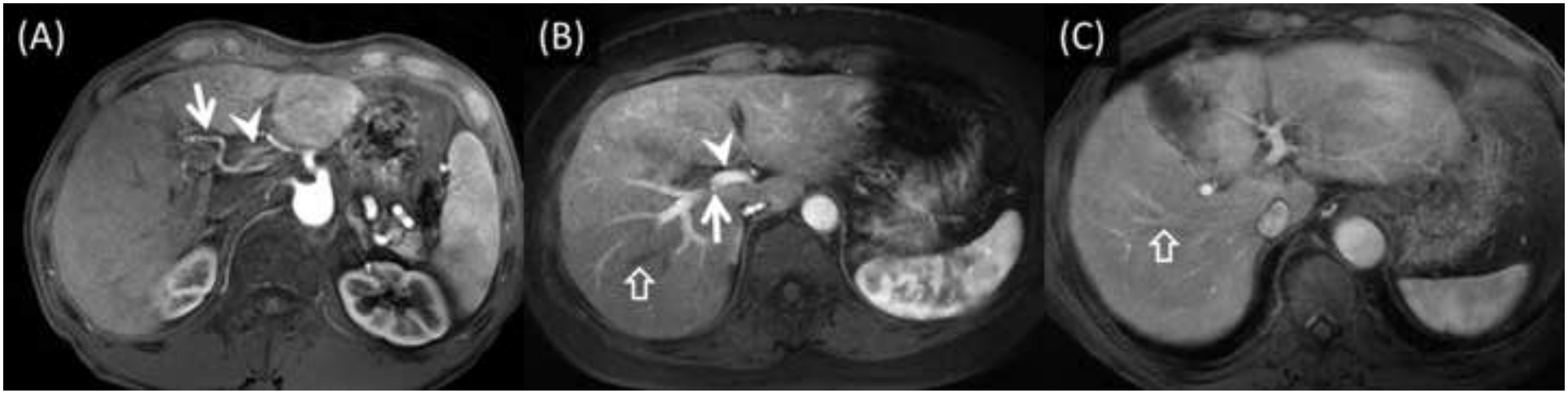

Figure 2

Click here to access/download;Figure;Figure2.tif

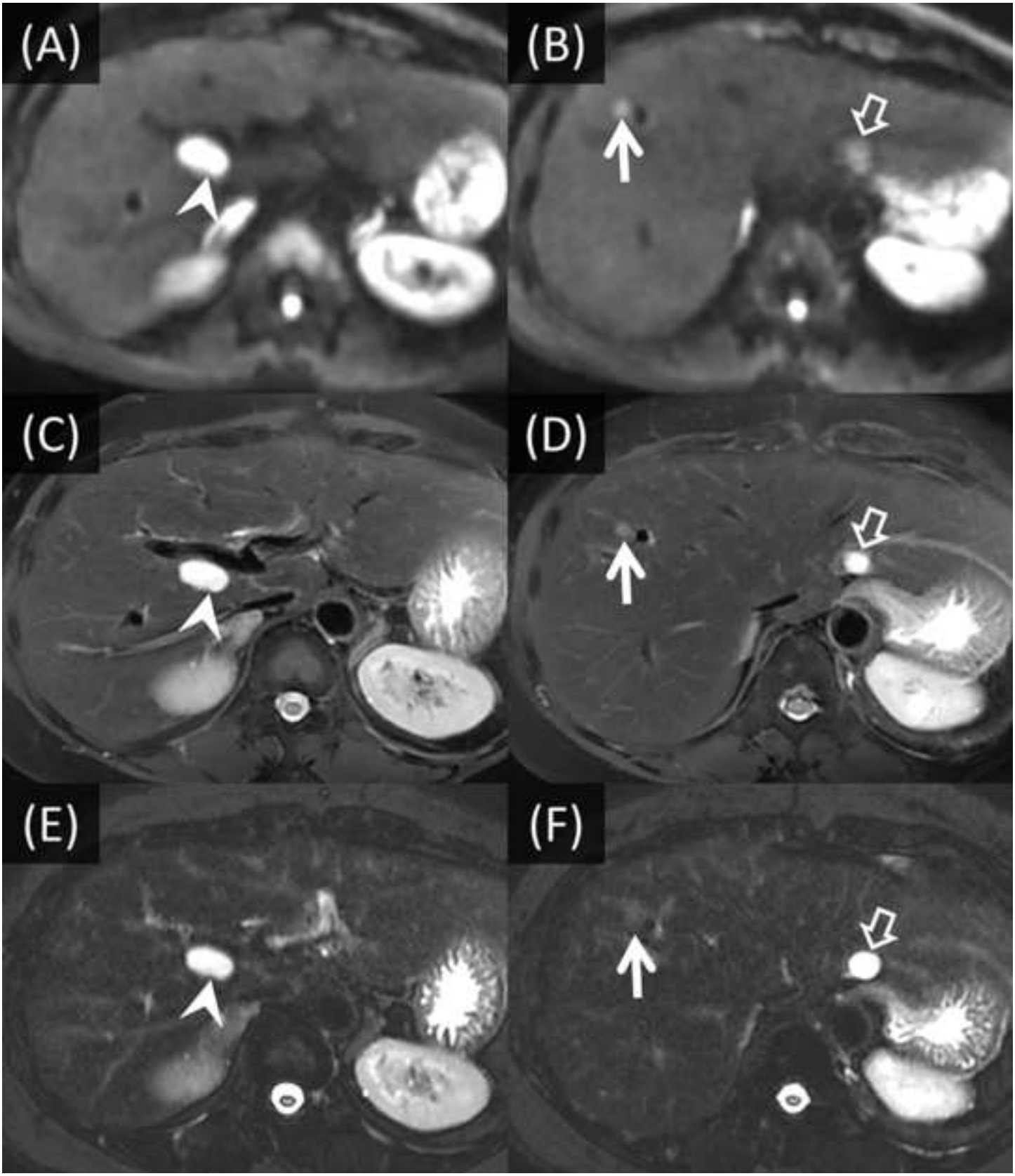

Figure 3

Click here to access/download;Figure;Figure3.tif

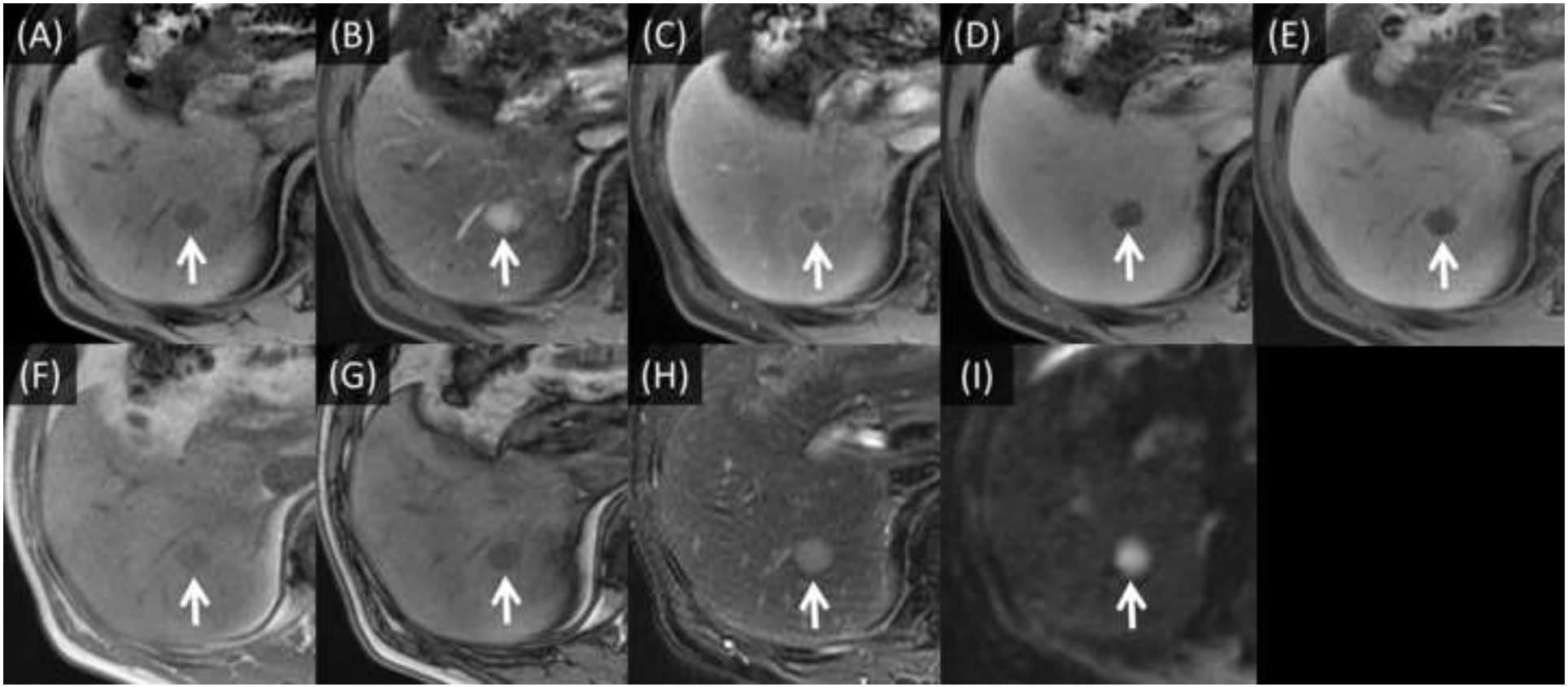

Figure 4

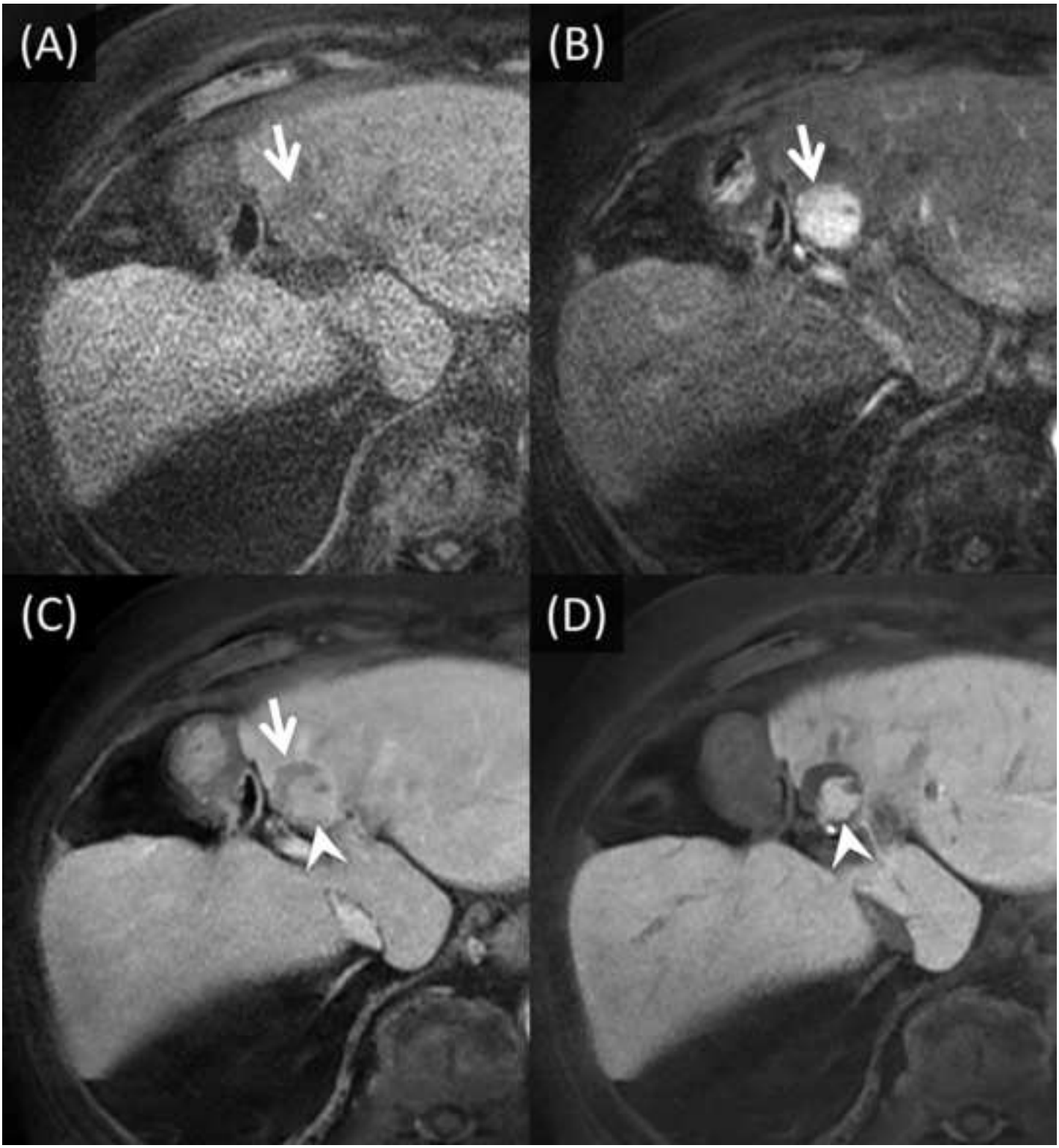

Figure 5

Click here to access/download;Figure;Figure5.tif

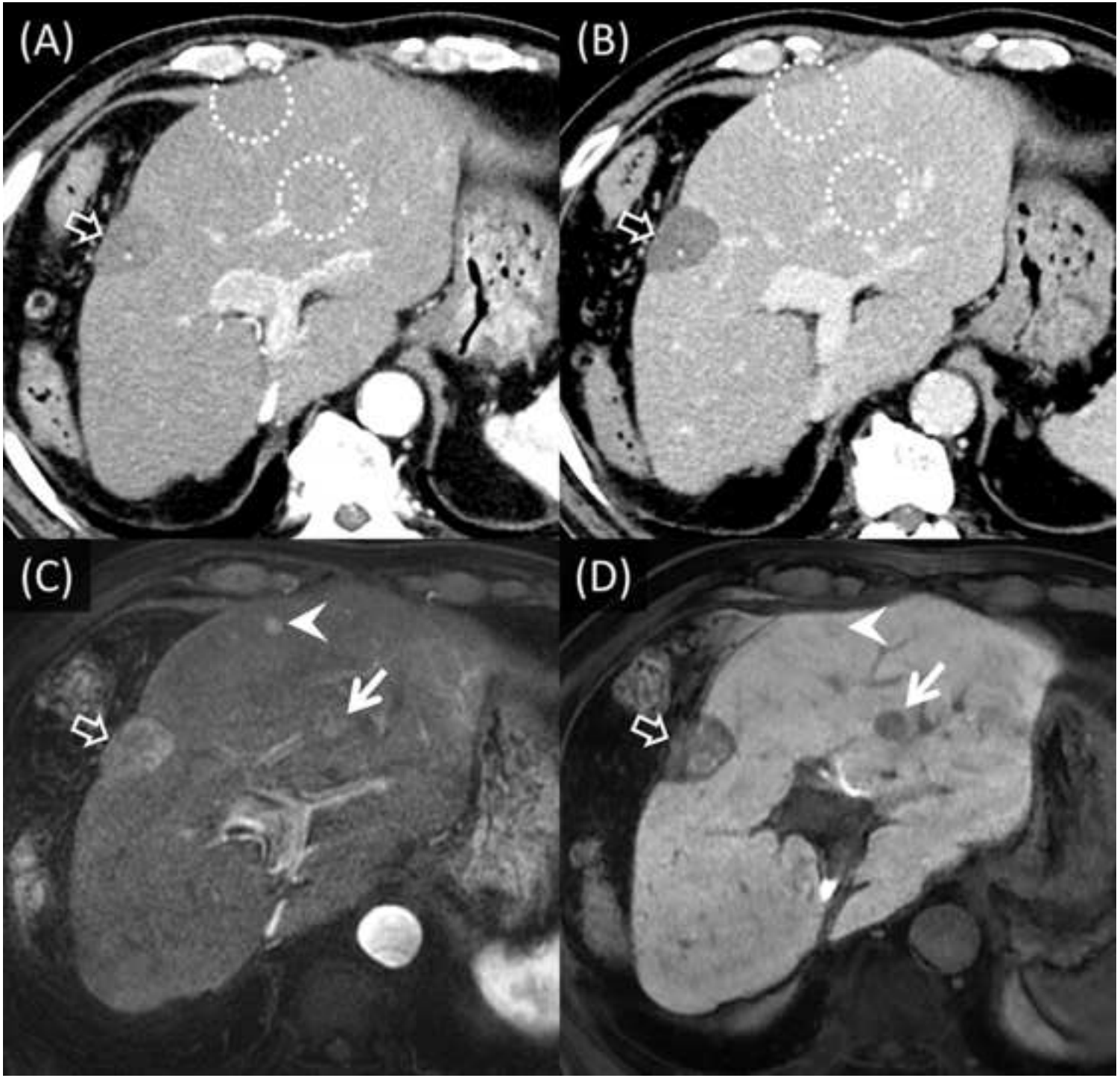

Figure 6

Click here to access/download;Figure;Figure6.tif

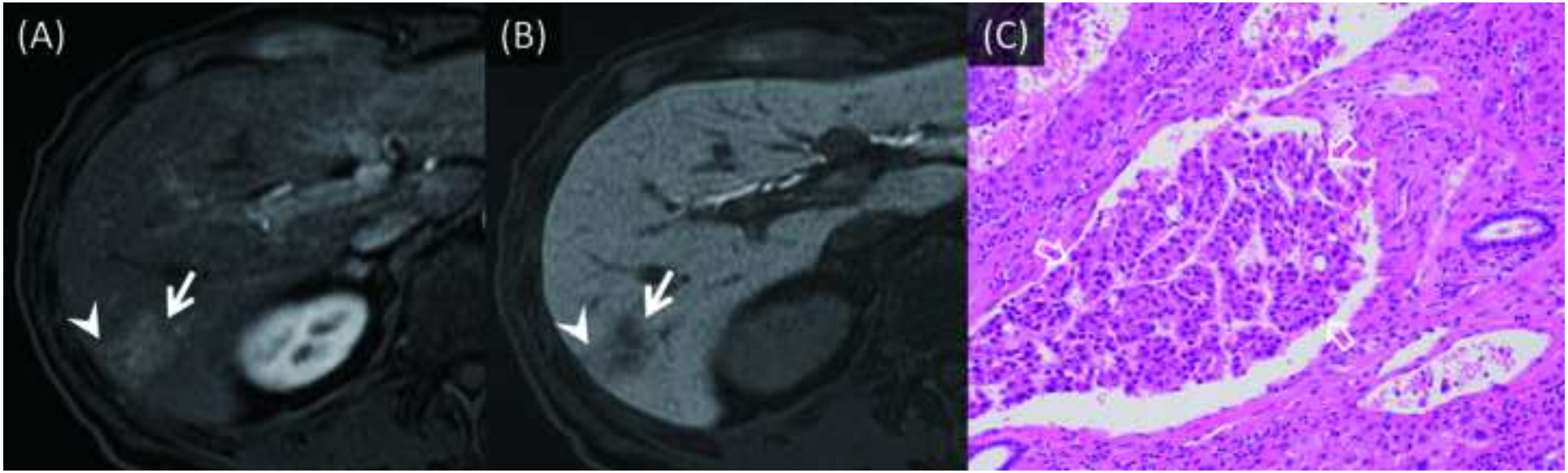

Figure 7

Click here to access/download;Figure;Figure7.tif

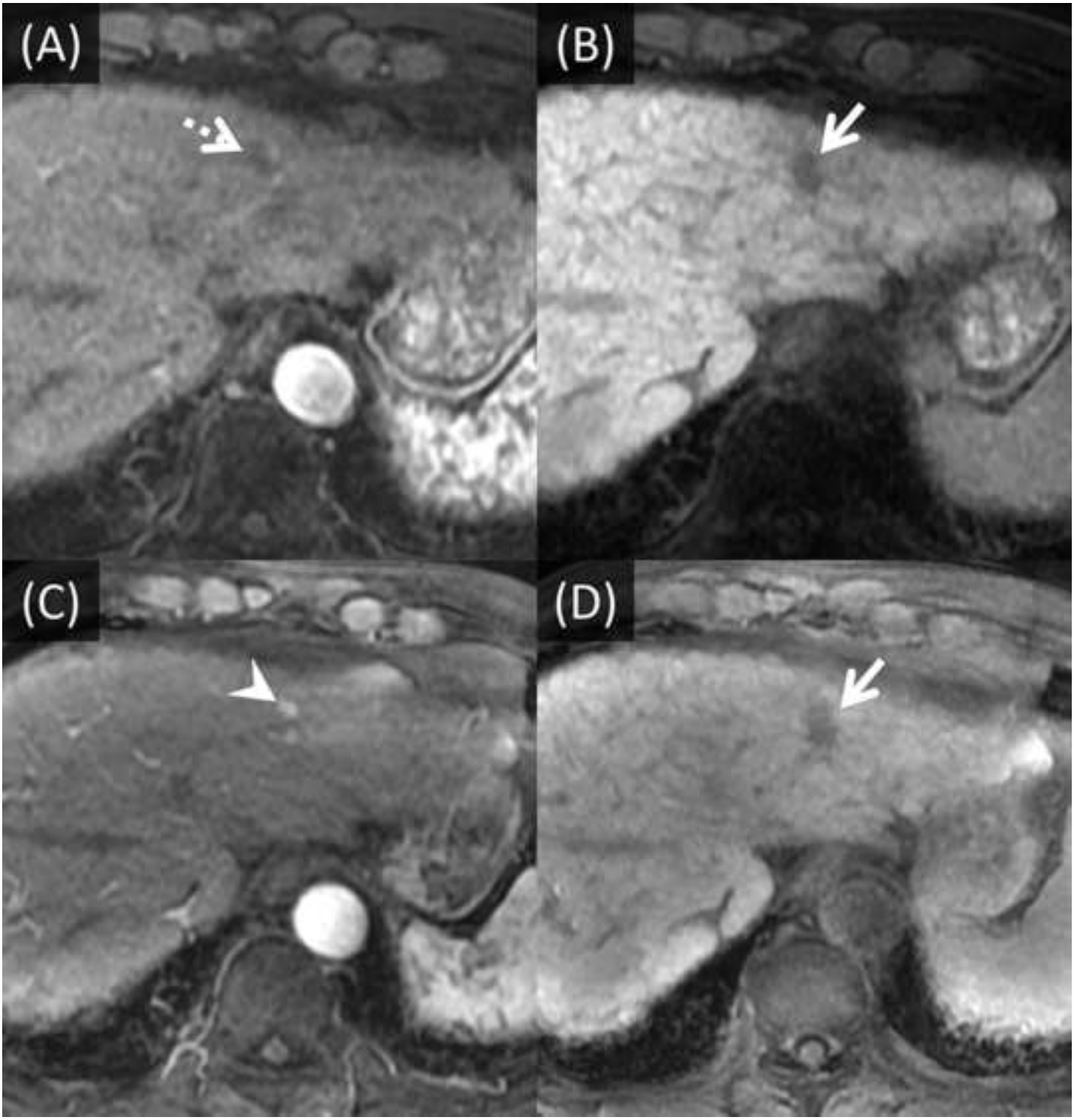

Figure 8

Click here to access/download;Figure;Figure8.tif

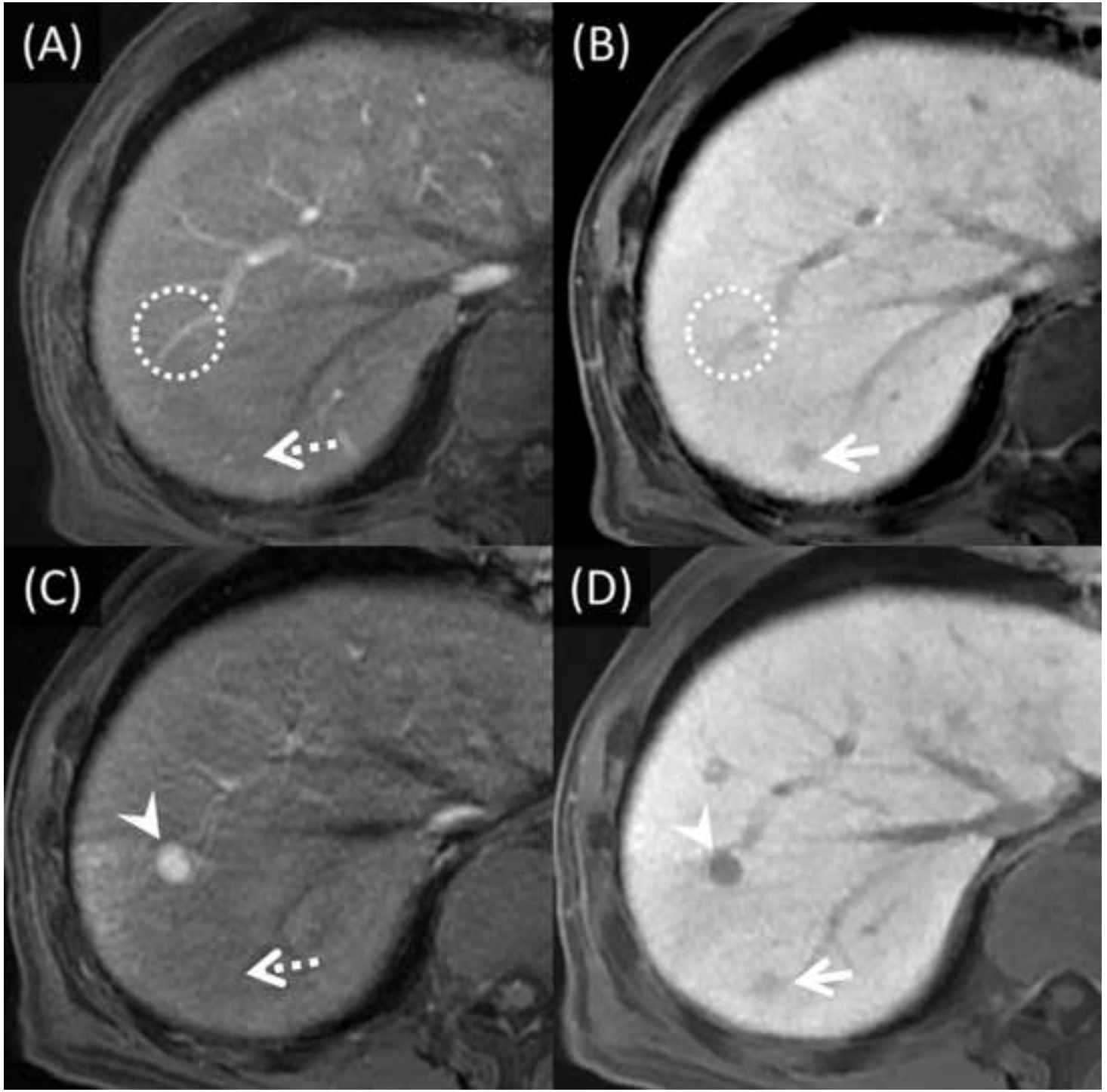

Figure 9

Click here to access/download;Figure;Figure9.tif

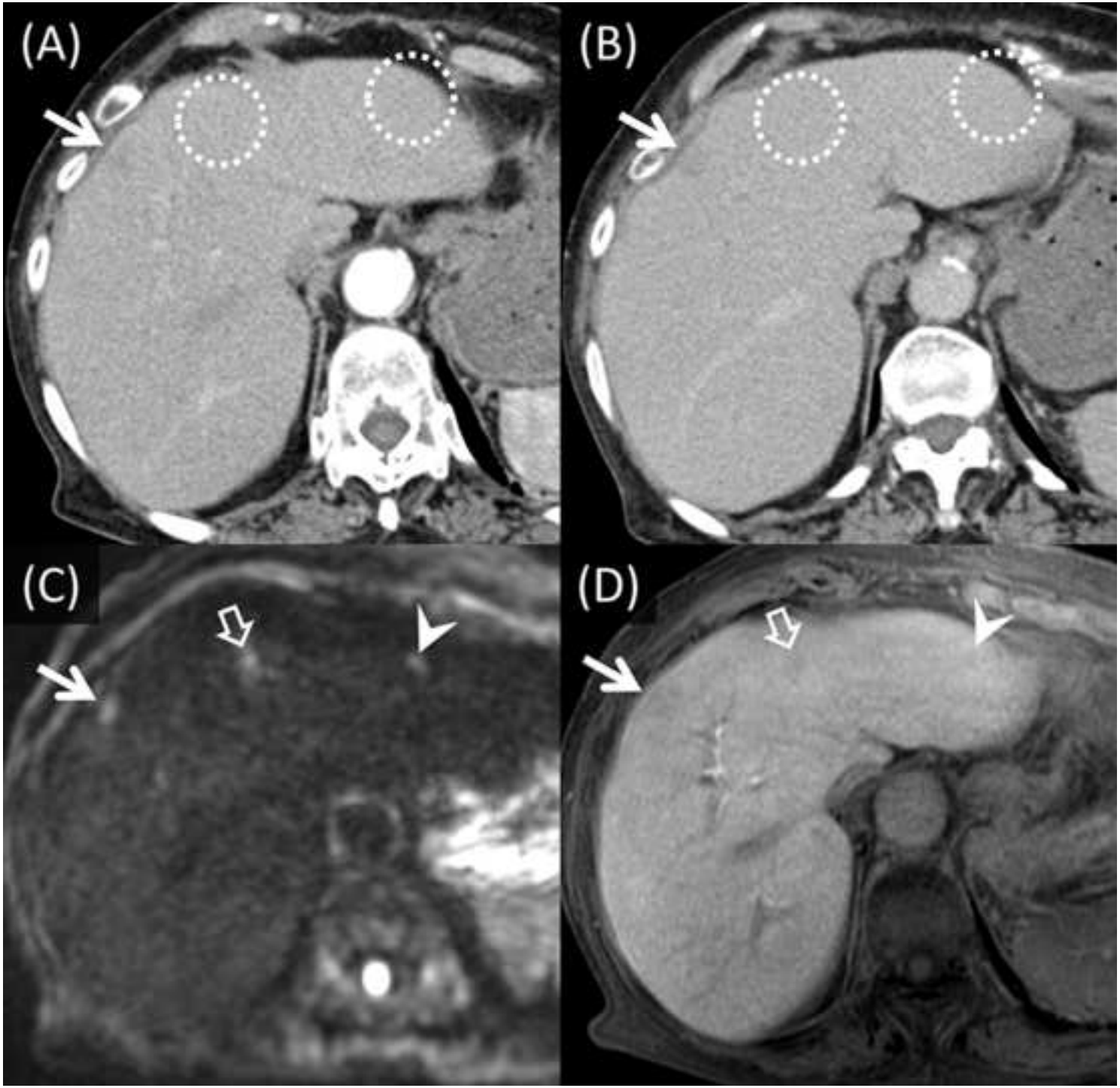

Figure 10

Click here to access/download;Figure;Figure10.tif

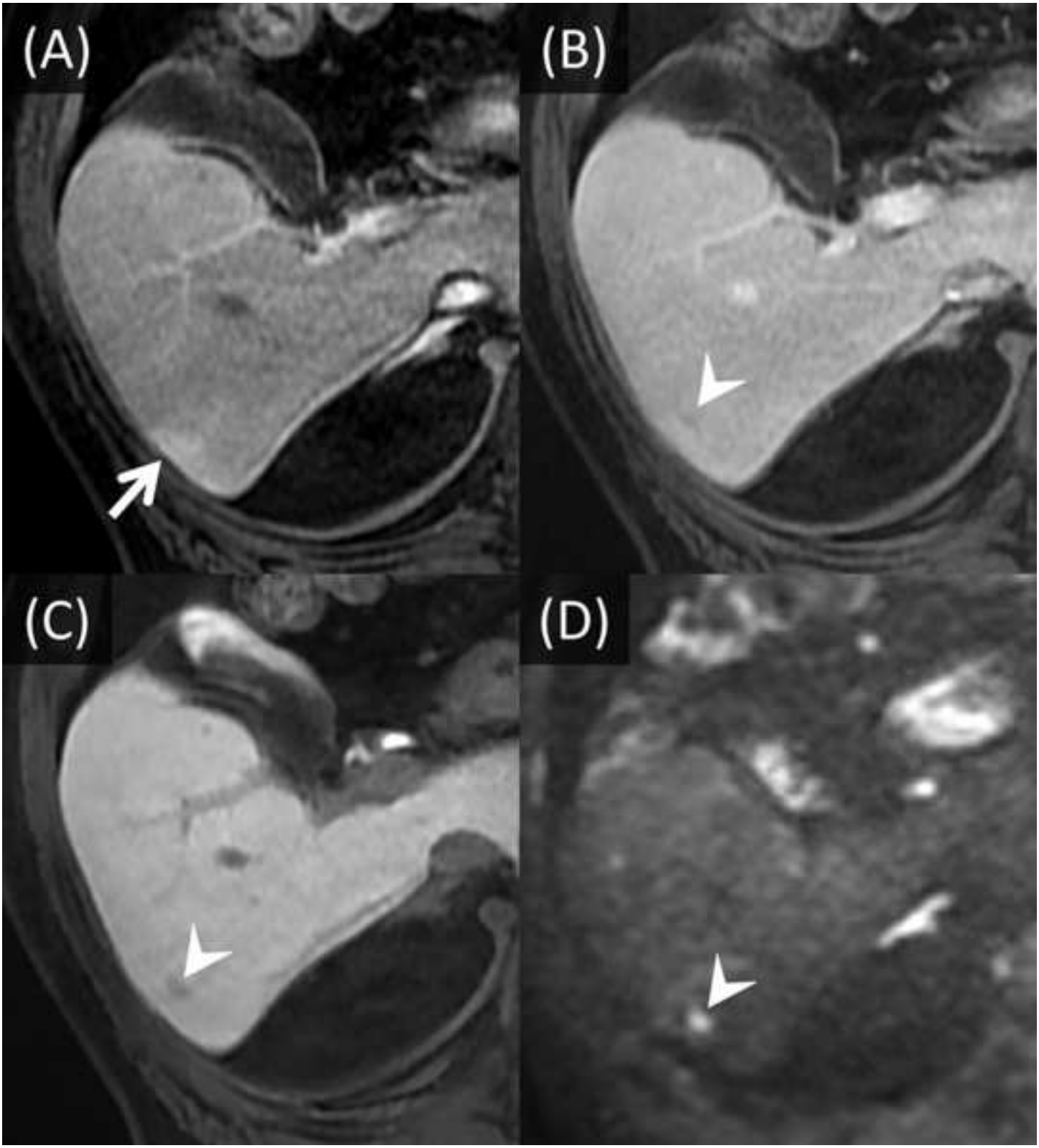

Figure 11

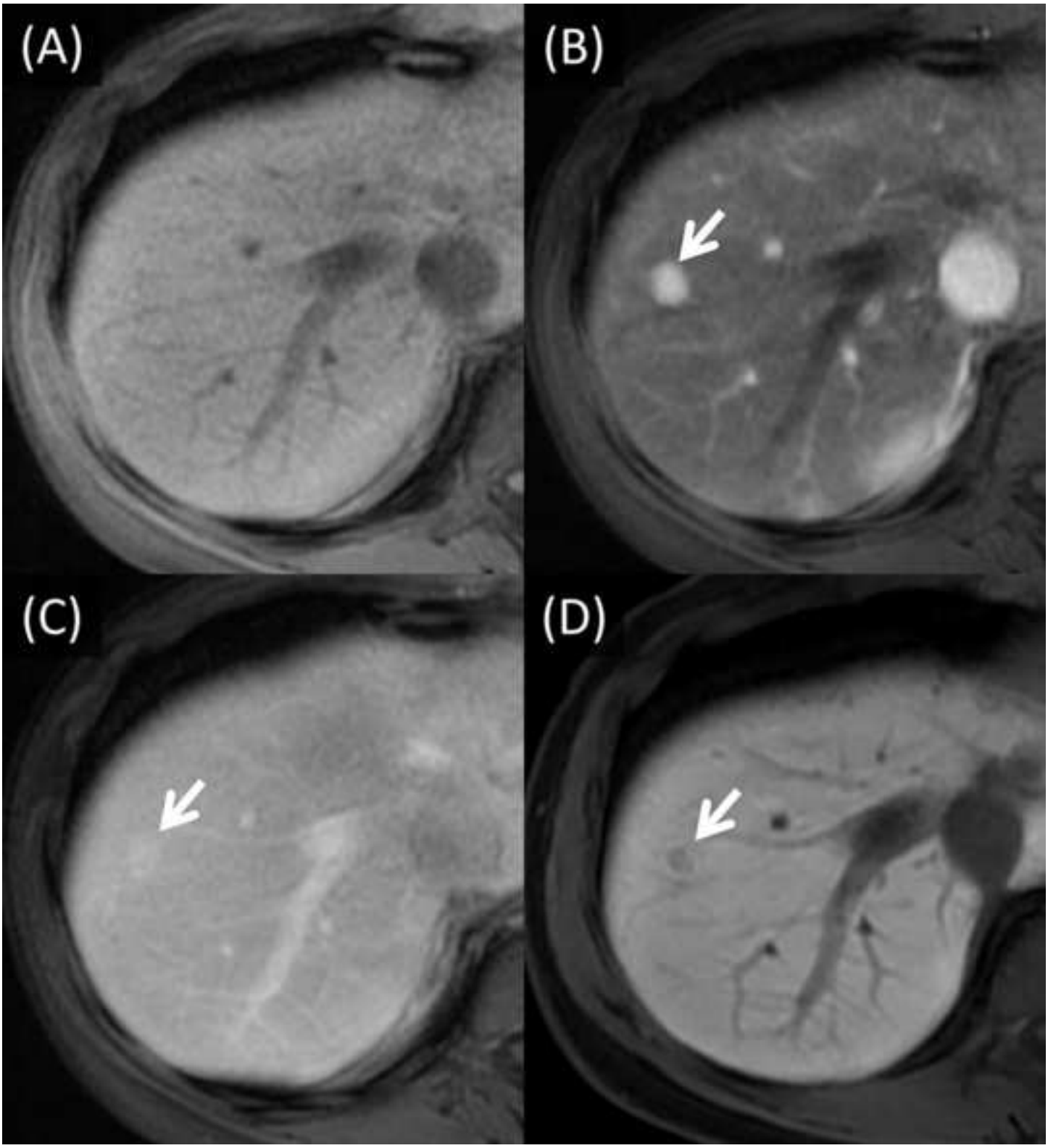

Figure 12

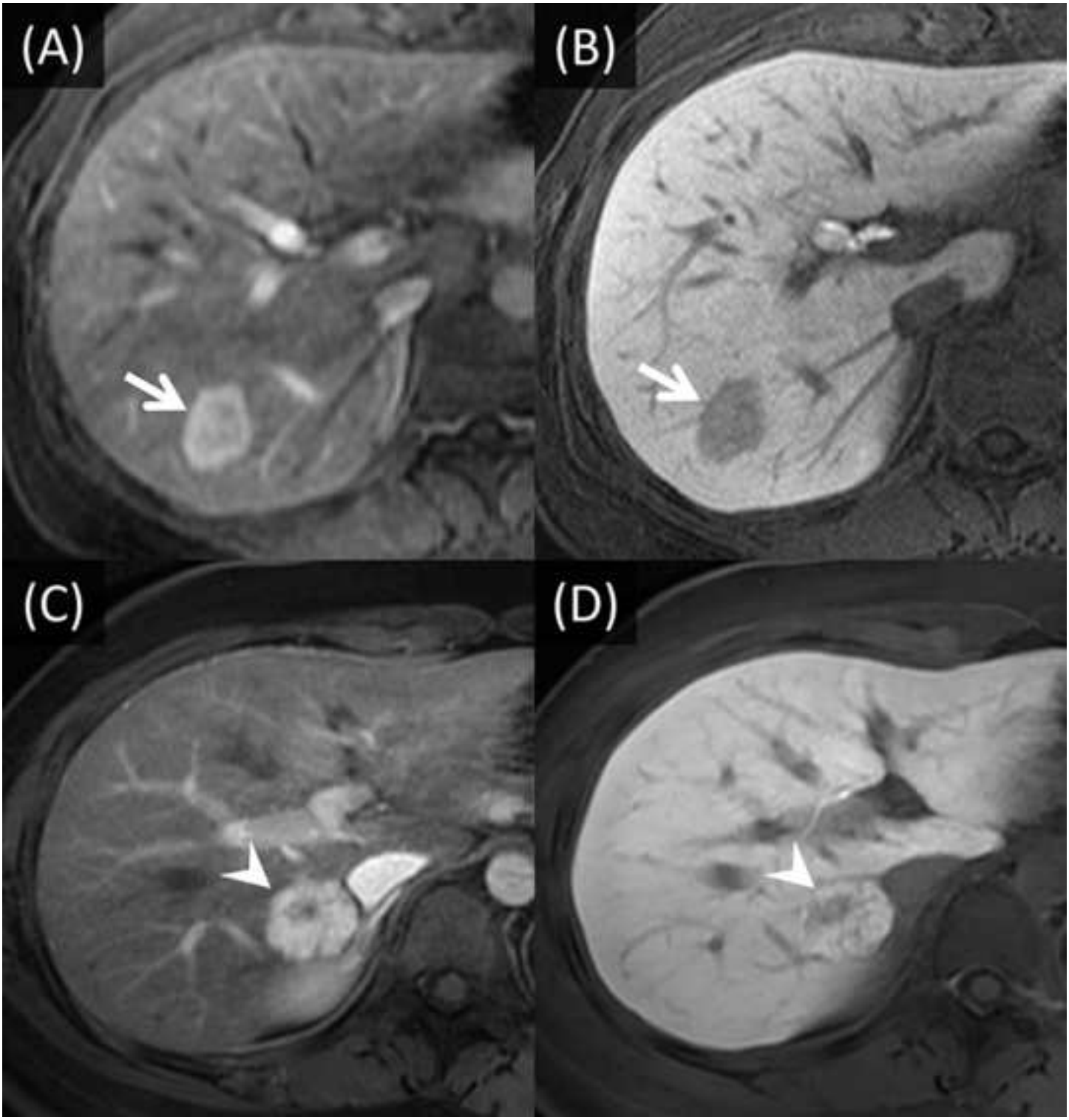

Figure 13

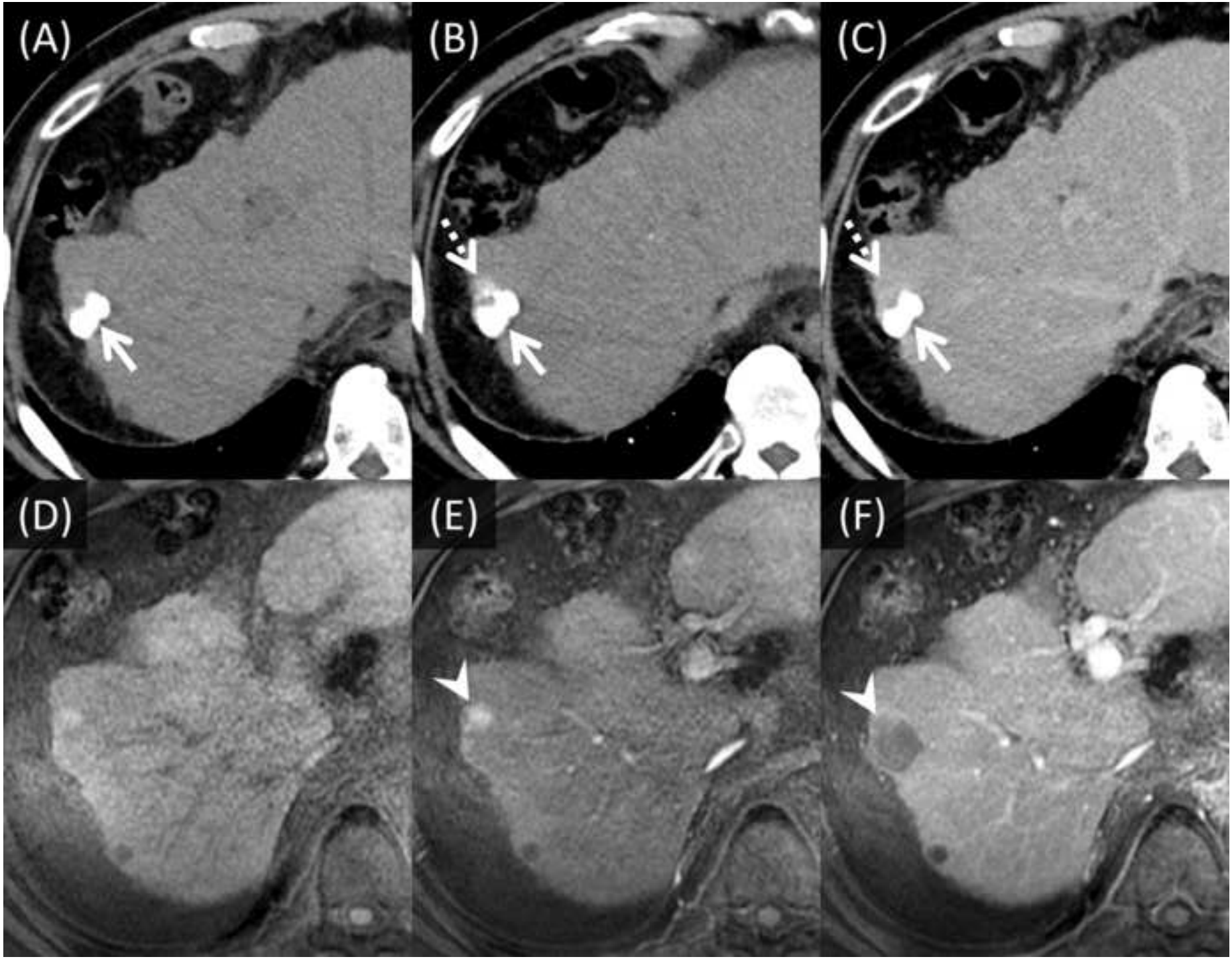

Figure 14

Click here to access/download;Figure;Figure14.tif

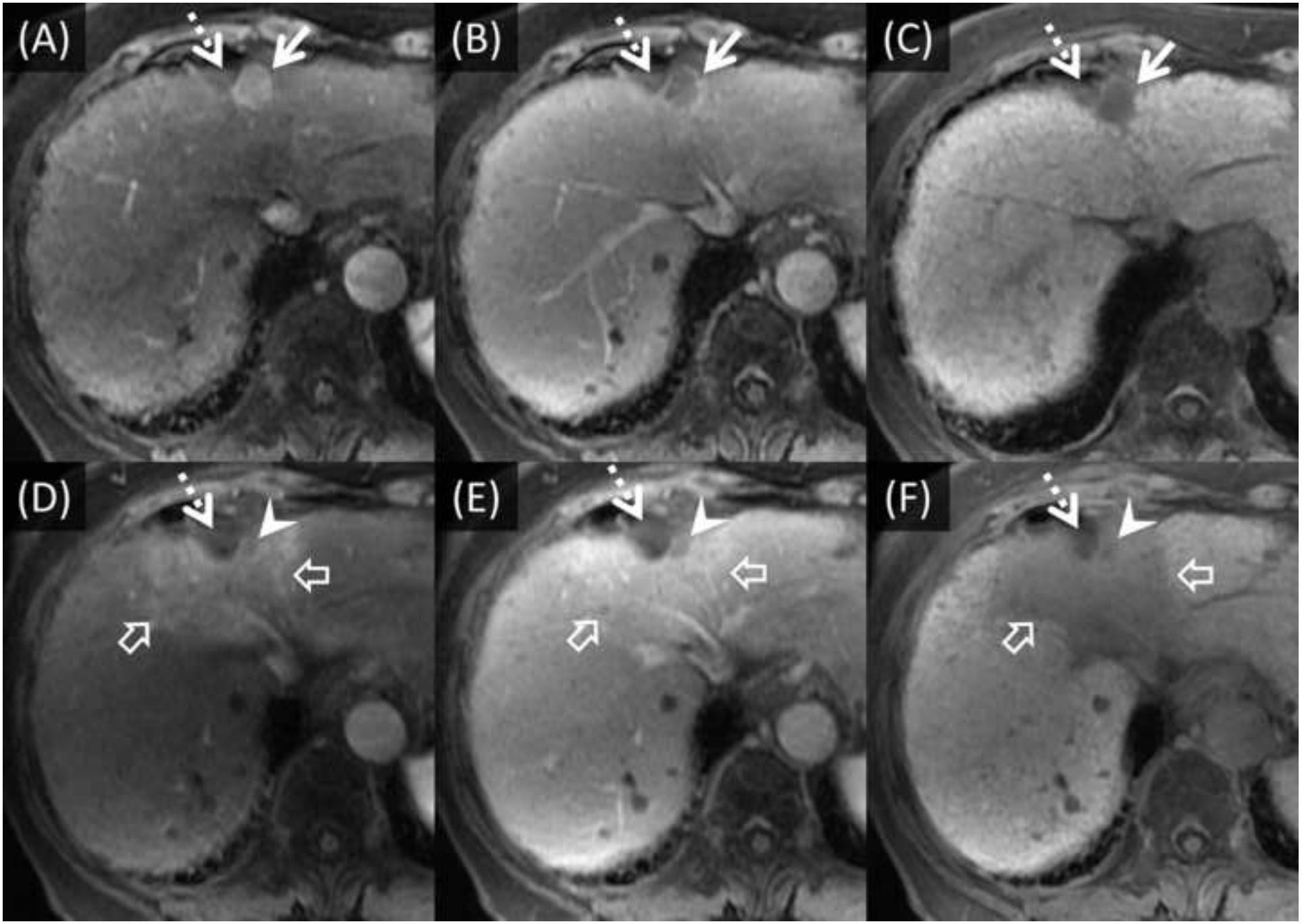

Figure 15

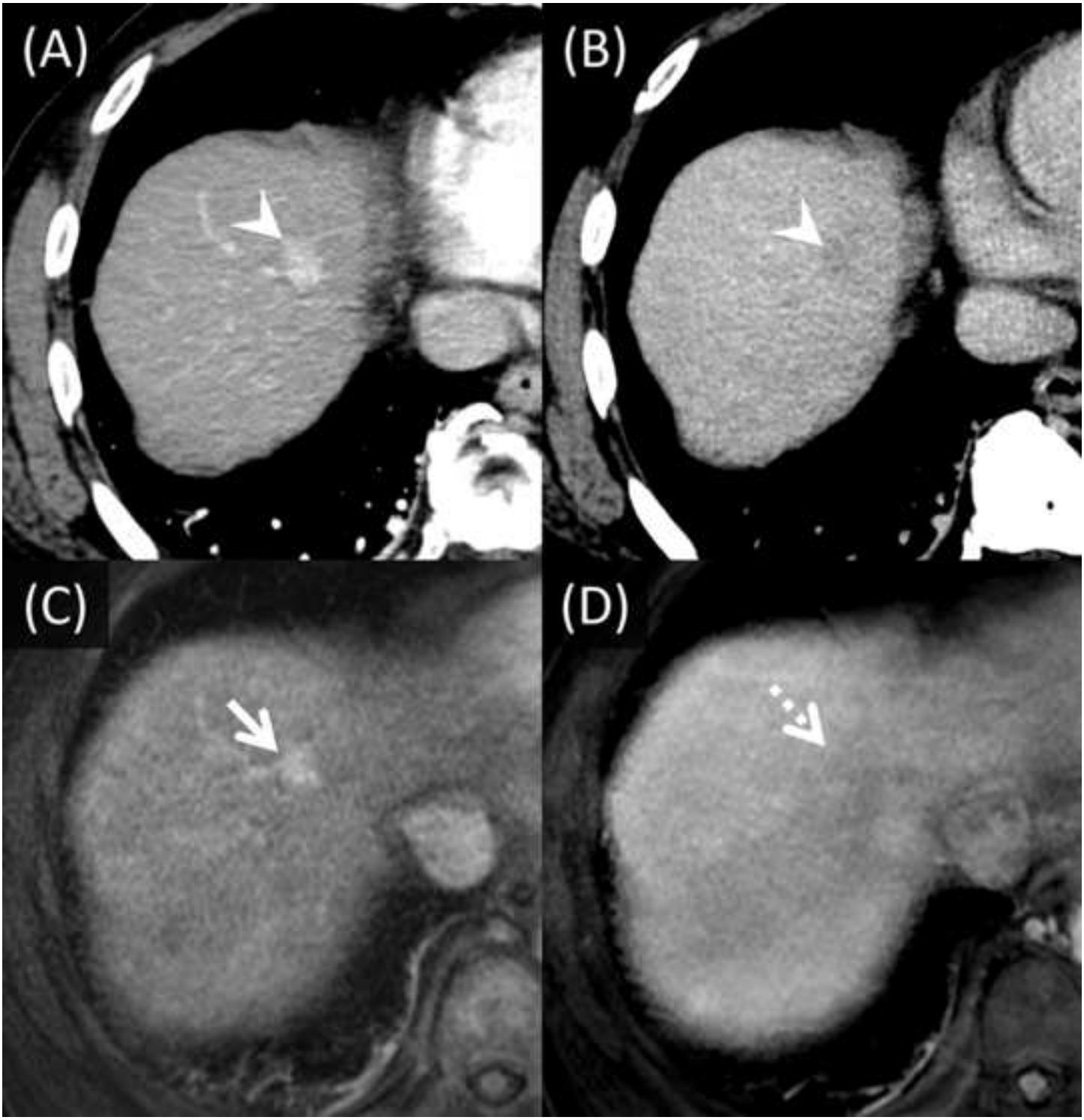

Figure 16

Click here to access/download;Figure;Figure16.tif

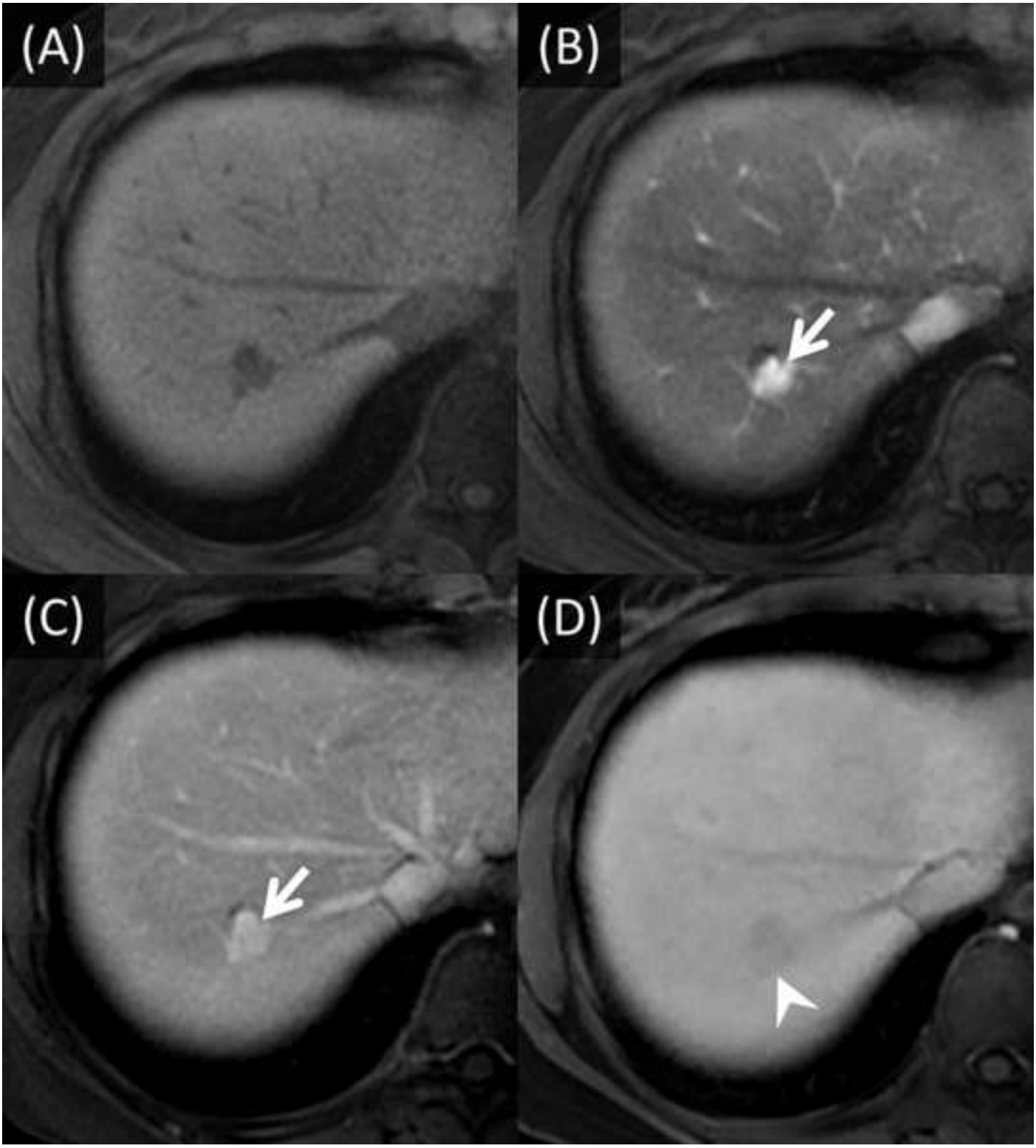

Figure 17

Click here to access/download;Figure;Figure17.tif